RESEARCH ARTICLE

Cadmium opens GluK2 kainate receptors with cysteine substitutions at the M3 helix bundle crossing

Timothy J. Wilding and James E. Huettner

Kainate receptors are ligand-gated ion channels that have two major roles in the central nervous system: they mediate a postsynaptic component of excitatory neurotransmission at some glutamatergic synapses and modulate transmitter release at both excitatory and inhibitory synapses. Accumulating evidence implicates kainate receptors in a variety of neuropathologies, including epilepsy, psychiatric disorders, developmental delay, and cognitive impairment. Here, to gain a deeper understanding of the conformational changes associated with agonist binding and channel opening, we generate a series of Cys substitutions in the GluK2 kainate receptor subunit, focusing on the M3 helices that line the ion pore and form the bundle-crossing gate at the extracellular mouth of the channel. Exposure to 50 µM Cd produces direct activation of homomeric mutant channels bearing Cys substitutions in (A657C), or adjacent to (L659C), the conserved SYT ANLAAF motif. Activation by Cd is occluded by modification with 2-aminoethyl MTS (MTSEA), indicating that Cd binds directly and specifically to the substituted cysteines. Cd potency for the A657C mutation (EC$_{50}$ = 10 µM) suggests that binding involves at least two coordinating residues, whereas weaker Cd potency for L659C (EC$_{50}$ = 2 mM) implies that activation does not require tight coordination by multiple side chains for this substitution. Experiments with heteromeric and chimeric channels indicate that activation by Cd requires Cys substitution at only two of the four subunits within a tetrameric receptor and that activation is similar for substitution within subunits in either the A/C or B/D conformations. We develop simple kinetic models for the A657C substitution that reproduce several features of Cd activation as well as the low-affinity inhibition observed at higher Cd concentrations (5–20 mM). Together, these results demonstrate rapid and reversible channel activation, independent of agonist site occupancy, upon Cd binding to Cys side chains at two specific locations along the GluK2 inner helix.

Introduction

Ionotropic glutamate receptors (iGluRs) are tetrameric proteins in the pore loop superfamily of ion channels that also includes voltage-gated sodium, calcium, and potassium channels as well as cyclic nucleotide–gated channels, TRP channels, and others (Hille, 2001). Structural analysis of iGluRs has revealed a modular organization with each subunit in the tetramer contributing to four distinct domains (Traynelis et al., 2010). The amino terminal domain (ATD) and ligand-binding domain (LBD) are extracellular. The transmembrane domain (TMD) forms the ion-conducting pore (Huettner, 2015), and the carboxy-terminal domain (CTD) is intracellular. In the closed state, tight association of inner helices at the bundle crossing occludes the conduction pathway, denying ions passage through the pore (Doyle et al., 1998; Sobolevsky et al., 2009). Conformational changes in the LBD contingent on agonist binding (Mayer, 2017; Twomey and Sobolevsky, 2018) open the channels by pulling on short linkers

that splay apart and deform the inner (M3) helix bundle to remove the occlusion and provide a route for water and ions into the central cavity (Chen et al., 2017; Twomey et al., 2017).

Despite limited overall sequence identity among iGluR subtypes (Traynelis et al., 2010), the bundle-crossing occlusion zone near the extracellular end of M3 comprises the longest identical segment across the different subunits. Throughout the paper we will use the numbering system in Fig. 1 A to refer to homologous M3 positions relative to the first conserved residue (S = 1) of the nine–amino acid SYTANLAAF motif. Initial evidence that the M3 helix plays a role in glutamate receptor gating came from analysis of the Lurcher mutant mouse in which an A to T point mutation at position 8 of this motif (A8T) in the orphan delta subunit results in constitutive channel activity (Zuo et al., 1997; Wollmuth et al., 2000). Subsequent work showed that substitution of the homologous A8 alanine residue in AMPA, kainate, and NMDA re-

Department of Cell Biology and Physiology, Washington University Medical School, St. Louis, MO.

Correspondence to James E. Huettner: jhuettner@wustl.edu.

ceptors increases apparent affinity for agonists, reduces desensitization, slows the rate of receptor deactivation, and allows some degree of constitutive channel opening in the absence of added agonist (Kohda et al., 2000; Taverna et al., 2000; Schwarz et al., 2001; Klein and Howe, 2004; Schmid et al., 2007). Interest in how this segment contributes to channel operation has been heightened by growing evidence that the LBD–TMD linkers and extracellular ends of M1, M3, and M4 serve as targets for a number of iGluR subtype-selective allosteric modulators (Yelshanskaya et al., 2016; Wang et al., 2017; Perszyk et al., 2018). In addition, recent studies have identified a spectrum of neuropathologies that can result from missense mutations at, or near, the Lurcher site of several human iGluR subunits (Li et al., 2016; Fernández-Marmiesse et al., 2018; Fry et al., 2018), including the kainate receptor subunit GluK2 (Guzmán et al., 2017). This accumulating evidence has spurred recent efforts to understand how spontaneous and engineered mutations in the bundle crossing and LBD–TMD linker segments affect iGluR function (Alsaloum et al., 2016; Yelshanskaya et al., 2017; Ladislav et al., 2018).

One approach to evaluating structural changes associated with channel gating involves cysteine scanning mutagenesis in which each amino acid in a protein segment is individually replaced with cysteine residues and the resulting set of mutant constructs tested for accessibility to modification by cysteine-reactive MTS reagents (Akabas, 2015). Differences in accessibility to MTS reagent modification, or in the rate of modification, between different gating states of the channel can thus provide information about the conformational changes that underlie the gating state transitions. In the course of these studies, it has sometimes been observed that cysteines substituted at specific locations allow fortuitous coordination of metal ions that can stabilize a specific conformational state (Liu et al., 1997; Holmgren et al., 1998; Zhou et al., 2015). In the case of iGluRs, a coordination site for copper ions that locks channels in the closed configuration can be formed by cysteine substitution at two distinct locations along the inner helix of NMDA receptor GluN1 (T3C) and GluN2 (L-1C) subunits (Sobolevsky et al., 2002). Both sites must be substituted in a heteromeric receptor in order for copper to bind, and recovery is slow without exposure to reducing agents (Sobolevsky et al., 2002). In addition, coapplication of Cd was shown to inhibit agonist-evoked current flow through homomeric GluA1 AMPA receptors with L-4C or A7C substitutions (Sobolevsky et al., 2004). Exposure to Cd in the absence of agonist had little effect, but recovery from inhibition was independent of agonist, suggesting that Cd did not become trapped when cells were switched to agonist-free solutions (Sobolevsky et al., 2004).

In the present study, we have examined the action of Cd on homomeric GluK2 kainate receptors with cysteine substitutions from W-8C to V12C near the extracellular end of the M3 helix. Our results show that exposure to Cd alone directly activates receptors with substitutions at two specific positions (A8C and L10C) within the bundle crossing occlusion zone. Furthermore, using chimeric subunits that combine the extracellular ATD and LBD from NMDA receptors with the GluK2 TMD and CTD (Wilding et al., 2014), we find that activation by Cd only requires cysteine substitution in two of the four subunits within a tetram-
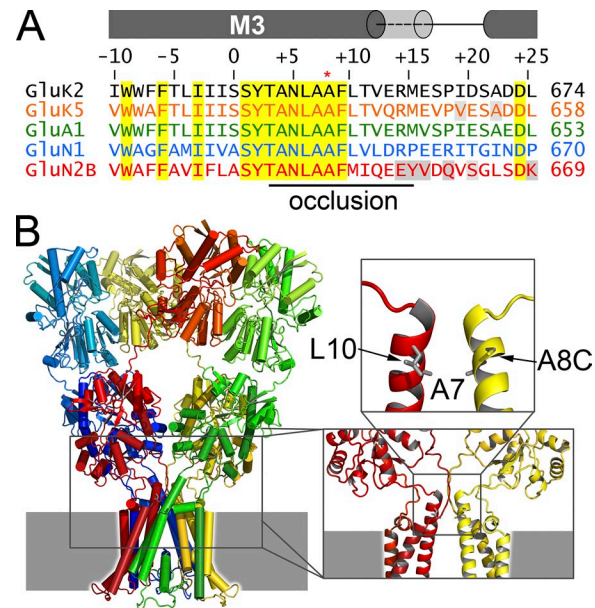

Figure 1. **The M3 helix sequence conservation. (A)** Alignment of ionotropic glutamate receptor subunit inner helix (M3) sequences. Numbers to the right denote position of the final residue from the N-terminal methionine. Homologous positions are numbered above the sequences relative to the first conserved residue (S = 1) of the nine–amino acid SYTANLAAF motif. Yellow highlights identical residues, and gray highlights positions of nonidentity within the GluN2 and GluK4/5 subfamilies. The A8 Lurcher site is marked with a red asterisk. In the closed conformation, the M3 helix extends to approximately +17 and +12 in the A/C and B/D configurations, respectively, as indicated by gray cylinders above the sequence. A horizontal line below the sequence indicates the closed conformation bundle crossing occlusion. **(B)** The GluK2 homology model based on the homomeric GluA2 AMPA receptor closed state x-ray structure. The A/C configurations are shown in green and blue; B/D configurations are shown in red and yellow. The bottom right box shows an expanded view of the linkage zone between the LBD and TMD of the B and D subunits. The top right box shows B and D subunit M3 helices with A8C and WT A7 and L10 side chains displayed.

eric receptor and that susceptibility to activation by Cd is essentially equivalent for cysteine substitutions to subunits in either the A/C or B/D conformation (Fig. 1).

Materials and methods
Complementary DNA (cDNA) constructs, cell culture, and transfection
WT GluK2(R) cDNA provided by Steve Heinemann (Salk Institute, La Jolla, CA) was subcloned into pcDNA3 for expression in human embryonic kidney (HEK293) cells. Conversion to glutamine at the Q/R site and cysteine substitutions along the GluK2 M3 helix were prepared as described (Wilding et al., 2008) using the QuickChange XL site-directed mutagenesis kit (Agilent Technologies). Additional subunit cDNAs provided by Mark Mayer (National Institutes of Health, Bethesda, MD), Peter Seeburg (Max Planck Institute, Heidelberg, Germany), and Stefano Vicini (Georgetown University, Washington, DC) were used to construct chimeric subunits as previously described (Wilding et al., 2014). Residue substitutions in chimeric subunits were generated by PCR. All constructs were verified by sequencing in the Washing-
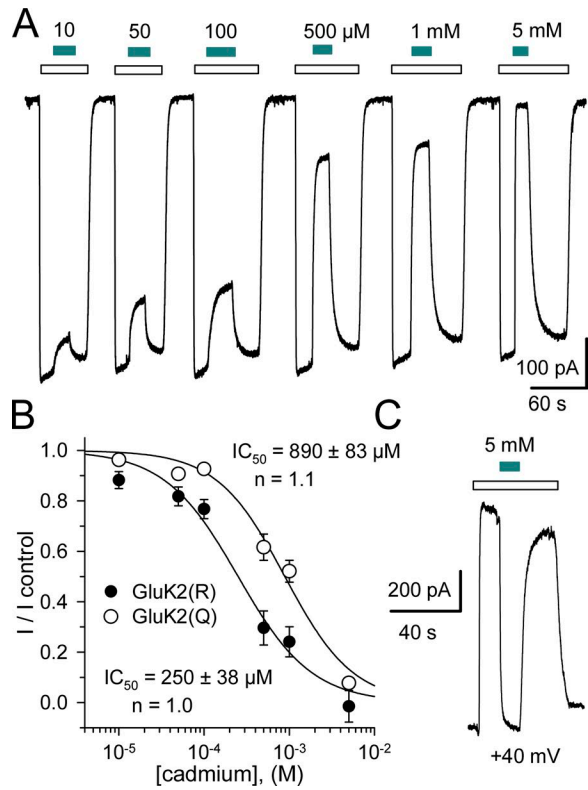
Figure 2. **Cd inhibits WT GluK2(Q) and GluK2(R). (A)** Whole-cell currents evoked by 10 µM kainate in an HEK cell transfected with GluK2(R). Kainate was applied as indicated by the open bars. Solid bars indicate coapplication of Cd at 10, 50, 100, and 500 µM and 1 and 5 mM. Holding potential is −80 mV. **(B)** Current (mean ± SEM) recorded during Cd coapplication plotted as a fraction of control current immediately before Cd exposure (five cells for Q and four cells for R). Smooth curves are the best fit of $I/I_{control} = 100/(1 + ([Cd]/IC_{50})^n)$, where IC_{50} is the concentration that produced half-maximal inhibition and n is the slope factor. **(C)** Outward current evoked by kainate in a different cell held at +40 mV was inhibited by brief exposure to 5 mM Cd as indicated by the solid bar.

ton University protein and nucleic acid chemistry laboratory. The HEK293 cells at ∼60% confluence were transfected with 1–3 µg of subunit cDNA using lipofectamine 2000 (Thermo Fisher Scientific). Coexpression of GFP from a second plasmid was used to identify transfected cells. On the day after transfection, cells were dissociated with mild protease treatment and replated at low density on nitrocellulose-treated 35-mm dishes (Wilding et al., 2008). Physiological recordings were obtained from green fluorescent cells 24–48 h after replating.

Electrophysiology

Cultures were perfused with Tyrode's solution (in mM): 150 NaCl, 4 KCl, 2 MgCl₂, 2 CaCl₂, 10 glucose, 10 HEPES, pH 7.4, with NaOH. Whole-cell electrodes were filled with internal solution (in mM): 140 Cs-glucuronate, 10 EGTA, 5 CsCl, 5 MgCl₂, 5 ATP, 1 GTP, 10 HEPES, pH adjusted to 7.4, with CsOH. Currents were recorded with an Axopatch 200A amplifier controlled by pClamp software (Molecular Devices). Agonist and Cd applications were made in control extracellular solution (160 mM NaCl, 2 mM CaCl₂ and 10 mM HEPES, pH 7.4, with NaOH) delivered by gravity-driven local perfusion from an eight-barreled pipette positioned near
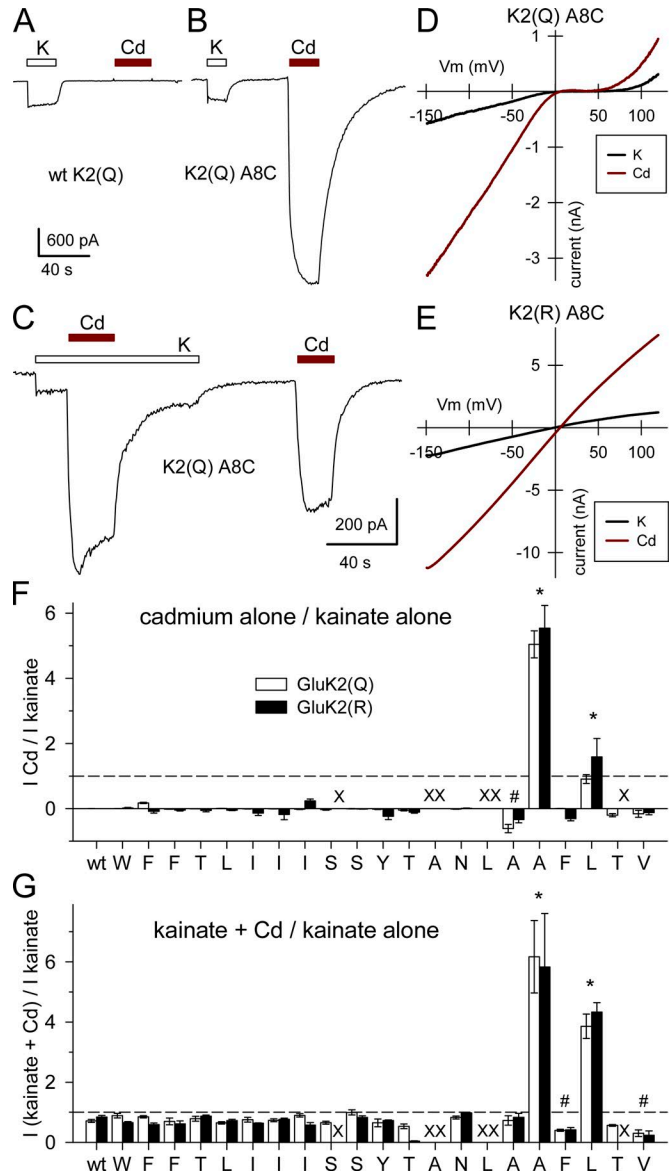

Figure 3. **Cd activates kainate receptors with inner helix cysteine substitutions. (A)** Whole-cell current evoked by 10 µM kainate (open bar) and no effect of 50 µM Cd alone (red bars) in an HEK cell transfected with WT GluK2(Q). **(B)** Currents evoked by exposure to kainate and Cd in a different cell transfected with GluK2(Q) A8C plotted at the same current scale. **(C)** Coapplication of 50 µM Cd and 10 µM kainate compared with Cd alone. In A–C, holding potential is −80 mV. **(D and E)** Current evoked by 10 µM kainate or 50 µM Cd during voltage ramps from −150 to +120 mV. **(F)** Current evoked by 50 µM Cd alone as a fraction of current evoked by 10 µM kainate alone (mean ± SEM, 4–114 cells per construct) for GluK2(Q) (open bars) and GluK2(R) (solid bars) WT or mutant, with Cys substitution at each position from W641C (−8) to V661C (+12). Crosses denote positions where exposure to either kainate or Cd failed to evoke any change in holding current. Symbols indicate current ratios significantly greater than (*) or less than (#) WT (P < 0.05, ANOVA on ranks, post hoc Dunn's test). **(G)** Current evoked by coapplication of Cd and kainate as a fraction of kainate alone (4–21 cells per construct).

the recorded cell (time constant for solution exchange ∼50–100 ms). All measurements were made relative to holding current in the control solution. Current–voltage (I-V) relations were generated and analyzed from triangle wave ramps as described (Lopez et al., 2013).
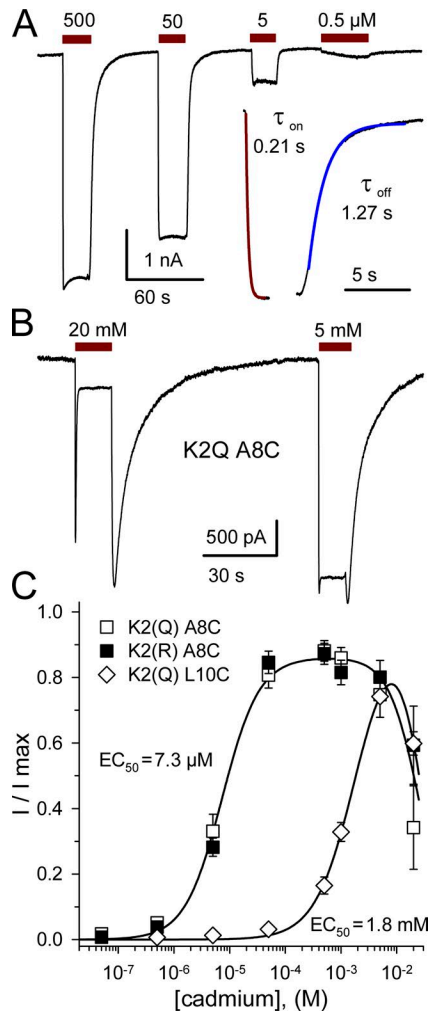
Figure 4. Concentration dependence of Cd activation. (A) Whole-cell currents evoked by 500, 50, 5, and 0.5 µM Cd alone in an HEK cell transfected with GluK2(Q) A8C. Inset shows exponential fits to the onset (red) and recovery (blue) phases of current evoked by 50 µM Cd shown on an expanded time scale. Holding potential is −80 mV. **(B)** Onset and recovery of low-affinity inhibition during exposure to 20 and 5 mM Cd in a different cell transfected with GluK2(Q) A8C. **(C)** Plot of steady-state current (mean ± SEM) as a fraction of the maximal Cd-evoked response. Smooth curve is the best simultaneous fit of $I/I_{max} = (m/(1 + (EC_{50}/[Cd])^n))/(1 + ([Cd]/IC_{50})^b)$ to the data for A8C substitution of both GluK2(Q) and GluK2(R), where $EC_{50} = 7.3 \pm 1.4$ µM and $IC_{50} = 25 \pm 5.4$ mM are the concentrations for half-maximal activation and inhibition, respectively; $n = 1.6 \pm 0.4$ and $b = 1.3 \pm 0.4$ are the slope factors; and $m = 0.86 \pm 0.03$ is the maximal steady-state current. Individual fits to Q (11 cells) and R (12 cells) data sets were not statistically superior by F test. Cd activated GluK2(Q) L10C with weaker potency ($EC_{50} = 1.8 \pm 0.3$ mM, $n = 1.2 \pm 0.2$; $IC_{50} = 26 \pm 7.1$ mM, $b = 1.9 \pm 0.5$; m set to 1; 12 cells).

Analysis

For concentration–inhibition experiments, the current recorded during exposure to agonist and Cd was plotted as a fraction of control current evoked by agonist alone. Concentration–inhibition results were fit with the following equation:

$$I/I_{control} = m + (1 - m)/(1 + ([Cd]/IC_{50})^n),$$

where IC_{50} is the Cd concentration producing half-maximal inhibition, n is the slope factor, and m is a baseline adjustment used when current during exposure to Cd was less than the holding current in control solution. Steady-state currents evoked by Cd were normalized to the maximal Cd response and fit with the following equation: $I/I_{max} = (1/(1 + (EC_{50}/[Cd])^n))/(1 + ([Cd]/IC_{50})^b)$, where I_{max} is the maximal current evoked by Cd; EC_{50} and IC_{50} are the Cd concentrations producing half-maximal activation and inhibition, respectively; and n and b are the slope factors for activation and inhibition.

Concentration dependence for chimeric subunits exhibiting both activation and inhibition by Cd was fit with $I/I_{max} = m + ((1/(1 + (EC_{50}/[Cd])^n) - m)/(1 + ([Cd]/IC_{50})^b))$, where EC_{50} and IC_{50} are the half-maximal concentrations for activation and inhibition, respectively; n and b are the slope factors or Hill coefficients for activation and inhibition; and m is the minimum current baseline. Coupling energies were calculated from EC_{50} values for double mutant cycles as follows (Kash et al., 2003; Gleitsman et al., 2008; Venkatachalan and Czajkowski, 2008):

$$\Omega\left(\Delta\Delta G\right) = -RT \ln\left[\frac{(EC_{50}\,wt * EC_{50}\,double\ mutant)}{(EC_{50}\,mutant\,1 * EC_{50}\,mutant\,2)}\right].$$

Unitary conductance was estimated as described previously (Wilding et al., 2008; Lopez et al., 2013) from plots of current variance versus mean current using data filtered at 2 kHz (−3 dB, four-pole Bessel) and digitized at 10 kHz during slow applications of agonist or Cd. Variance was calculated for 100-ms intervals after subtracting a straight line fit to correct for steady amplitude changes (Bean et al., 1990). When open probability (P_o) is low (∼0.2 or less), the variance versus mean plot is approximately linear with slope equal to the unitary current (Bean et al., 1990; Lingle, 2006). For $P_o > 0.2$, the relationship of variance (σ^2) to mean current (I) is parabolic: $\sigma^2 = i * I - I^2 /N$, where i is the estimated unitary current, and N is the estimated number of channels (Sigworth, 1980). Maximal P_o was estimated from $P_o = I_{max}/(i * N)$.

Results are reported as mean ± SEM, and significance was assigned for $P < 0.05$. One-way and two-way ANOVA and t tests were performed with SigmaStat (Systat Software). Curve fits using different numbers of parameters were evaluated by the ratio of residual variance test, F statistic (Swartz et al., 1992).

Modeling

We used Modeller version 9.18 (Eswar et al., 2008) with two-fold symmetry constraints for the A/C and B/D conformations to model GluK2(R) A8C on the homomeric GluA2 open state structure (PDB accession no. 5WEO) from the Sobolevsky laboratory (Twomey et al., 2017). Structures are displayed with PyMol. Kinetic model simulations were performed in Excel by numerical integration of entry and exit rate equations for each postulated state.

Online supplemental material

Fig. S1 shows Cd activation of GluK2(Q) A8C receptors that include a second mutation in the LBD that reduces agonist potency (Mah et al., 2005). Fig. S2 illustrates inhibition of GluK2 A8S, T, Y, or F by increasing concentrations of Cd. Fig. S3 shows kinetic model simulations that reproduce several features observed for activation and inhibition of receptors with A8C substitutions to

Table 1. **Half-maximal concentrations for Cd activation and inhibition**

Construct	EC$_{50}$ (µM)	Slope, n	IC$_{50}$ (mM)	Slope, b	Cells (no.)
K2(Q) WT (KA-evoked)			0.89 ± 0.08	1.1 ± 0.1	5
K2(R) WT (KA-evoked)			0.25 ± 0.04	1.0 ± 0.1	4
K2(Q&R) A8C	7.3 ± 1.4	1.6 ± 0.4	25 ± 5.4	1.3 ± 0.4	23
K2(Q) L10C	1,800 ± 300	1.2 ± 0.2	26 ± 7.1	1.9 ± 0.5	12
N1/K2 A8C + N2B/K2 A8C	5.6 ± 1.7	0.9 ± 0.1	1.1 ± 0.2	1.8 ± 0.4	21
N1/K2 A8C + N2B/K2	47 ± 8	1.0 ± 0.2	13 ± 10	0.9 ± 0.4	14
N1/K2 + N2B/K2 A8C	27 ± 9	0.9 ± 0.1	1.1 ± 0.2	1.8 ± 0.4	14

one or both chimeric subunit. Table S1 provides a summary of parameters derived from these simulations.

Results

Cd inhibits WT GluK2(Q) and GluK2(R)

Previous work showed that WT native and recombinant kainate receptors are potently inhibited by the trivalent ions La and Gd with an IC$_{50}$ of ~3 µM (Huettner et al., 1998). In contrast, divalent cations including Ni, Co, Cu, Cd, and Zn have a substantially weaker inhibitory effect on WT kainate receptors, typically causing <50% inhibition at 100 µM (Huettner et al., 1998; Mott et al., 2008; Veran et al., 2012). Before evaluating the effect of Cd on Cys substitution mutants, we determined the concentration dependence of inhibition at homomeric recombinant kainate receptors expressed in HEK293 cells after transfection of cDNA encoding WT GluK2. As shown in Fig. 2, exposure to Cd produced dose-dependent inhibition of whole-cell currents mediated by homomeric GluK2 with either glutamine (Q) or arginine (R) at the Q/R editing site. Average current evoked by 10 µM kainate was –2.0 ± 0.9 nA (R) and –2.8 ± 0.5 nA (Q), and inhibition by Cd was somewhat more potent at GluK2(R) than at GluK2(Q) with half-maximal values of 250 ± 38 µM and 890 ± 83 µM, respectively (five cells for Q and four cells for R). In a few cells, we also tested for possible voltage dependence of Cd inhibi-

tion by coapplication of Cd and kainate at a holding potential of +40 mV where current flows outward through kainate receptor channels. As shown in Fig. 2 C, Cd coapplication produced essentially equivalent inhibition at positive holding potentials as was observed at –80 mV (Fig. 2, A and B), indicating a lack of voltage dependence and suggesting that Cd binding responsible for inhibition does not occur within the conduction pathway (Huettner et al., 1998; Mott et al., 2008). In addition, exposure to 50 µM Cd alone caused no significant change in the holding current recorded from untransfected cells or in cells transfected with WT GluK2(Q) or GluK2(R) (Fig. 3 A).

Cd activates GluK2(Q) and GluK2(R) with Cys substitutions at specific residues

Previous studies have analyzed NMDA (Beck et al., 1999; Jones et al., 2002; Yuan et al., 2005; Sobolevsky et al., 2007; Chang and Kuo, 2008) and AMPA (Sobolevsky et al., 2004) receptors with Cys substitutions in the M3 transmembrane helix and linker to the S2 extracellular segment. To test for commonalities among iGluRs, we generated a series of point mutations along the M3 helix of both edited (R) and unedited (Q) GluK2 kainate receptor subunits, scanning from W641C (–8) to V661C (+12; Fig. 1). Homomeric receptors with Cys substitutions at most locations were functional when expressed by transient transfection in HEK293 cells as determined by activation of whole-cell current during

Table 2. **Time constants for Cd activation and inhibition**

| Construct	Activation (s)		Cells (no.)	[Cd]	Inhibition (s)		Cells (no.)	[Cd]
	Tau on	Tau off			Tau on	Tau off		
GluK2 WT (KA-evoked)					0.51 ± 0.10	2.49 ± 0.48	8	5 mM
GluK2 A8C	0.81 ± 0.06	8.41 ± 1.07	94	50 µM				
	0.10 ± 0.01	9.91 ± 3.10	19	20 mM	0.33 ± 0.04	0.60 ± 0.07	19	20 mM
K2(Q) L10C	0.71 ± 0.15	1.52 ± 0.25	16	1 mM				
N1/K2 A8C + N2B/K2 A8C	0.90 ± 0.23	5.95 ± 0.91	35	50 µM				
	0.10 ± 0.01	8.68 ± 2.73	11	5 mM	0.39 ± 0.05	1.12 ± 0.13	11	5 mM
N1/K2 A8C + N2B/K2	0.88 ± 0.13	2.91 ± 0.63	30	50 µM				
	0.11 ± 0.02	1.87 ± 0.12	13	5 mM	0.37 ± 0.05	0.67 ± 0.06	13	5 mM
N1/K2 + N2B/K2 A8C	0.97 ± 0.17	3.24 ± 0.60	33	50 µM				
	0.09 ± 0.02	3.91 ± 0.87	10	5 mM	0.22 ± 0.02	0.66 ± 0.06	10	5 mM
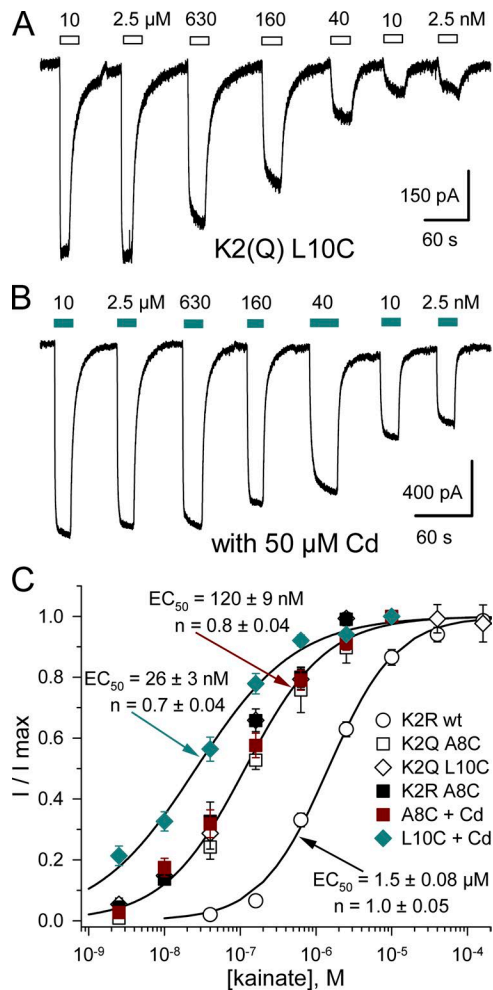
Figure 5. **The M3 Cys substitutions increase agonist potency, and Cd coapplication has a differential effect on L10C versus A8C. (A)** Whole-cell currents evoked by decreasing concentrations of kainate (open bars) from 10 μM to 2.5 nM in an HEK cell transfected with GluK2(Q) L10C. **(B)** In a different cell, the same agonist concentrations were applied together with 50 μM Cd (cyan bars). Note the increased responses to low doses. **(C)** Plots of current evoked by kainate (mean ± SEM) normalized to the maximal response for each condition. Smooth curve is the best fit of $I/I_{max} = 1/(1 + (EC_{50}/[kainate])^n)$, where EC_{50} is the concentration for half-maximal activation and n is the slope factor. Activation of WT receptors is half-maximal at 1.5 μM (data taken from Wilding et al., 2005). Homomeric M3 A8C or L10C substitution increased kainate potency by ~12.5-fold. Individual fits to the results for K2(Q) A8C (5 cells), K2(R) A8C (3 cells), and K2(Q) L10C (10 cells) were not significantly better than the simultaneous fit to all three data sets with $EC_{50} = 120 ± 9$ nM and $n = 0.8 ± 0.04$. Coapplication of 50 μM Cd to K2(Q) L10C (nine cells) produced an additional increase in apparent agonist potency of ~4.5-fold ($EC_{50} = 26 ± 3$ nM), whereas agonist potency was unchanged with coapplication of 0.5 μM Cd to K2(Q) A8C (nine cells).

exposure to 10 μM kainate. Only the A4C and L6C mutants failed to function in both the Q and R form, whereas the S0C and T11C substitutions were functional in the Q but not the R form. In addition to kainate, each of the Cys substitution mutants were tested with exposure to 50 μM Cd alone (Fig. 3, B, C, and F) and 50 μM Cd together with 10 μM kainate (Fig. 3, C and G). Consistent with our results for WT receptors (Figs. 2 and 3 A), Cd had little or no effect when applied alone and caused modest (~10–40%) inhibition of current evoked by kainate (Huettner et al., 1998) in cells

transfected with most of the mutant constructs (Fig. 3, F and G). However, exposure to Cd produced substantially different effects for receptors with Cys substitutions at a few specific M3 locations. In particular, exposure to Cd alone significantly reduced the holding current in cells expressing GluK2 subunits with A7C substitution (Fig. 3 F) and activated large currents in cells transfected with A8C or L10C substitution mutants (Fig. 3).

For receptors with A8C or L10C substitutions, the currents activated by kainate or by Cd alone displayed similar I-V relations (Fig. 3, D and E). As for WT GluK2(Q) and GluK2(R), the I-V relations recorded for kainate and for Cd alone in cells expressing homomeric GluK2(Q)A8C (Fig. 3 D) or L10C showed prominent rectification, owing to pore block by cytoplasmic polyamines (Traynelis et al., 2010). In contrast, the I-V relations were nearly linear in cells transfected with the A8C (Fig. 3 E) or L10C mutations of GluK2(R), which resists polyamine block (Traynelis et al., 2010). Together, these results provide strong evidence that currents evoked by exposure to Cd arise from direct activation of mutant channels and not from some indirect effect enabled by mutant subunit expression. Moreover, the rectification observed for unedited (Q) receptors demonstrates that Cys substitution at A8 or L10, as well as Cd activation of mutant receptors, does not perturb the elements required for polyamine block, as can occur with M3 residue substitutions closer to the central cavity (Wilding et al., 2010).

Bar plots in Fig. 3, F and G, summarize the action of 50 μM Cd alone or together with 10 μM kainate on the series of M3 Cys substitutions. On average, for the A8C substitution, the current evoked by Cd was similar in amplitude to current elicited by kainate plus Cd, suggesting that 50 μM Cd alone achieves nearly maximal activation. By contrast, for the L10C substitution, currents evoked by coapplication of Cd and kainate (Fig. 3 G) were substantially larger on average than the sum of currents activated by Cd alone and kainate alone (Fig. 3 F), suggesting synergy between Cd and kainate in promoting channel activation for this substitution.

To determine the concentration dependence of Cd activation, we recorded currents evoked by 0.5 μM to 20 mM Cd in cells transfected with the A8C substitution in GluK2(Q) or GluK2(R) or with the GluK2(Q) L10C mutant. As shown in Fig. 4, Cd activated both the edited (R) and unedited (Q) forms of the A8C substitution mutant with half-maximal potency of ~10 μM (Table 1). Separate fits to the data points for Q and R isoforms were not statistically superior to the simultaneous fit of both datasets shown in Fig. 4 C (F test, P > 0.05). A second measure of Cd affinity came from exponential fits to the onset (τ_{on}) and recovery (τ_{off}) phases of currents evoked by 50 μM Cd (Fig. 4 A, inset, and Table 2). For the simplest model in which activation results from binding a single Cd: $K_d = \tau_{on} * [Cd]/(\tau_{off} - \tau_{on})$, where the dissociation constant (K_d) is estimated to be 11.2 ± 1.3 μM (87 cells). The potency for Cd activation was substantially weaker for the L10C than the A8C substitution mutant of GluK2, as judged either by the higher L10C mutant Cd EC_{50} of 1.8 ± 0.3 mM (Fig. 4 C) or the K_d of 1.7 ± 0.7 mM (16 cells) estimated from onset and recovery time constants of currents evoked by 1 mM Cd. At the highest Cd doses tested, homomeric channels with either A8C or L10C substitutions exhibited partial inhibition of steady-state currents (Fig. 4,
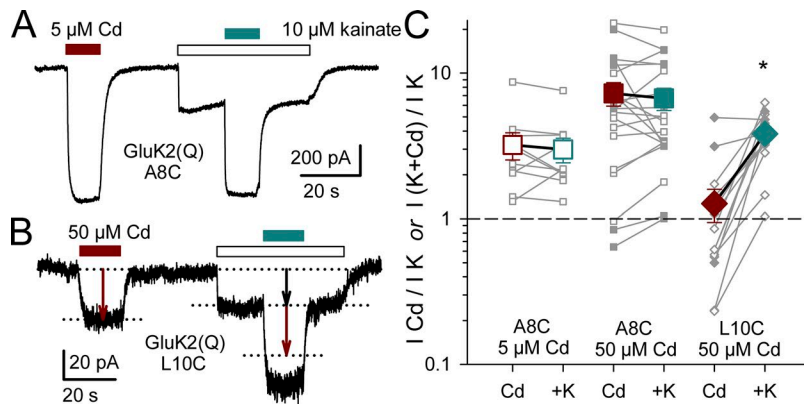
Figure 6. **Synergistic activation by Cd and kainate at GluK2 L10C. (A and B)** Whole-cell currents evoked by Cd alone (red bars), 10 µM kainate (open bars), or kainate plus Cd (cyan bars) in HEK cells expressing GluK2(Q) A8C (A) or GluK2(Q) L10C (B). Note that for the L10C substitution (B), current evoked by kainate plus Cd was larger than the sum of current evoked by kainate alone (black arrow) and Cd alone (red arrow). **(C)** Currents evoked by Cd alone and kainate plus Cd in the same cell plotted as a fraction of the current evoked by kainate alone for GluK2 A8C with either 5 µM Cd (open symbols, 10 cells for Q) or 50 µM Cd (20 cells; 13 for Q and 7 for R) and GluK2 L10C with.50 µM Cd (15 cells; 10 for Q and 5 for R). Results for individual cells are plotted in gray and connected by lines (open symbols are Q, and solid symbols are R); larger colored symbols plot mean ± SEM. Note the y-axis log scale. Asterisk denotes significant difference from Cd alone (P < 0.00003, paired *t* test).

B and C, and see below); however, inhibition of mutant receptors exhibited substantially weaker potency than for homomeric WT receptors (Fig. 2 and Table 1).

A8C and L10C substitutions increase agonist potency

Previous work has shown that inner helix mutations, including A8 substitutions (Kohda et al., 2000; Taverna et al., 2000; Klein and Howe, 2004), can increase iGluR agonist potency, highlighting the mechanistic linkage between agonist binding to the LBD and conformational changes at the bundle crossing. To determine whether A8C and/or L10C substitutions affected agonist potency at GluK2, we recorded currents evoked by 2.5 nM to 160 µM kainate in cells transfected with GluK2(Q) A8C, GluK2(R) A8C, and GluK2(Q) L10C. As shown in Fig. 5, kainate was >10-fold more potent at receptors with A8C or L10C substitution as compared with WT (Jones et al., 1997; Wilding et al., 2005). Indeed, the concentration dependence for all three constructs was similar enough that individual fits to data for each one alone were not statistically superior to a simultaneous fit of all three data sets with an EC$_{50}$ = 120 ± 9 nM (F test; Fig. 5).

In addition to recording currents evoked by kainate alone, we also evaluated currents elicited by kainate together with a low dose of Cd (Fig. 5), either 50 µM for the L10C substitution or 0.5 µM for the A8C substitution. These values were chosen near the "foot" of the respective concentration–response relations for current activation by Cd alone (Fig. 4). For receptors with the L10C substitution, adding 50 µM Cd caused an ∼4.5-fold increase in kainate potency (EC$_{50}$ = 26 ± 3 nM); however, for the A8C substitution, adding 0.5 µM Cd caused no significant change in EC$_{50}$ for activation by kainate (Fig. 5 C). In addition, for the A8C substitution, we did not observe evidence for synergy between 10 µM kainate and submaximal doses of Cd (0.5 or 5 µM). Currents evoked by coapplication of kainate and 0.5 or 5 µM Cd in cells expressing GluK2 A8C were less than or equal in amplitude to the sum of current evoked by kainate alone and Cd alone (Fig. 6, A and C), whereas for L10C, coapplication of kainate plus Cd evoked current that was larger than the sum of current elicited by kainate alone and Cd alone (Fig. 6, B and C).

To determine whether the increase in agonist potency observed for receptors with M3 Cys substitutions (Fig. 5) was somehow required for activation by Cd, we added an E to D sub-

stitution in the LBD (E738D) that was previously found to reduce agonist potency (Mah et al., 2005). As shown in Fig. S1, current activation by 50 µM Cd alone persisted in the GluK2(Q) A8C E738D double mutant despite a substantial reduction in kainate potency (EC$_{50}$ = 28 ± 5 µM). Thus, Cd activation is not restricted to receptors with higher agonist affinity. Indeed, the ∼230-fold change in EC$_{50}$ from 120 nM for K2(Q) A8C to 28 µM for K2(Q) A8C E738D is similar in magnitude to the 270-fold change previously reported for K2(Q) E738D compared with WT GluK2 (Mah et al., 2005). Based on these agonist EC$_{50}$ values (Kash et al., 2003; Gleitsman et al., 2008; Venkatachalan and Czajkowski, 2008), we estimate a coupling energy (ΔΔG) <100 cal/mol for the A8C and E738D mutations, suggesting a lack of strong interaction between the residues at these two positions.

Cd opens the channel

Previous work suggests that iGluRs with amino acid substitutions at the A8 Lurcher site exhibit lower unitary conductance than WT receptors (Kohda et al., 2000; Murthy et al., 2012). In addition, editing at the Q/R site reduces conductance of WT GluK2(R) <1 pS, making it difficult to resolve unitary currents above the background noise (Howe, 1996; Huettner, 2015). Therefore, to provide an initial characterization of channel activity promoted by exposure to Cd, we performed fluctuation analysis (Lopez et al., 2013) of whole-cell currents evoked by 50 and 500 µM Cd or 10 µM kainate in cells expressing edited (R) receptors with A8C substitution, as well as currents evoked by 10 µM kainate plus 50 µM Cd in cells transfected with GluK2(Q) L10C (Fig. 7).

For the L10C substitution, most plots of current variance (σ²) versus mean current (I) followed a parabolic trajectory (Sigworth, 1980): σ² = i × I – I²/N, where i and N are the estimated unitary current and number of channel, respectively (Fig. 7 and Table 3). Cd alone, kainate alone, and Cd plus kainate activated channels with similar estimated unitary conductance (∼1 pS), and differences in maximal current amplitude between Cd, kainate, and Cd plus kainate largely reflected differences in open probability: P$_o$ = I$_{max}$/(i ∗ N). On average, for GluK2(Q) L10C, the unitary conductance with Cd was at least 80% of that for kainate, while the ratio of open probability with Cd to kainate (P$_o$ Cd/P$_o$ K) was 0.4 ± 0.1 for 50 µM Cd alone, 1.7 ± 0.5 for 500 µM Cd alone, and 3.9 ± 1.3 for kainate plus 50 µM Cd (Table 3).
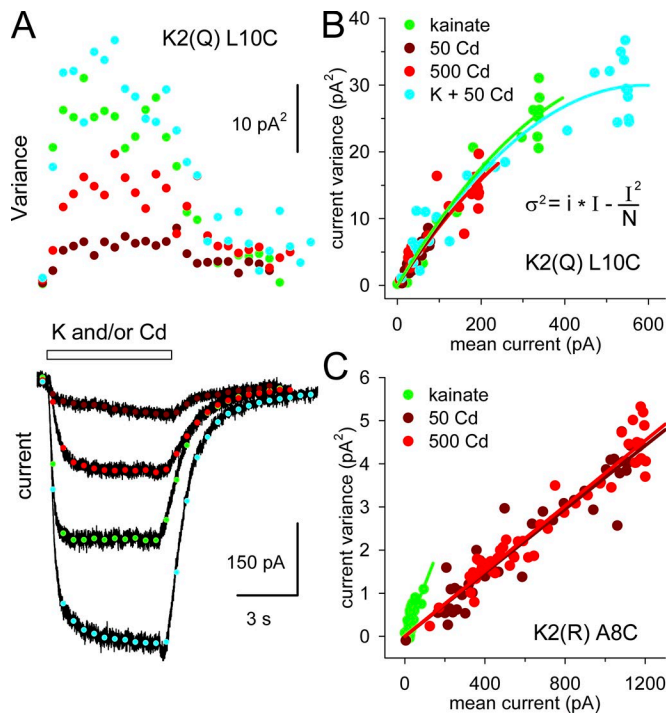
Figure 7. **Cd increases open probability. (A)** Points show mean current (bottom) and current variance (top) for whole-cell responses evoked by 50 and 500 µM Cd (dark and bright red, respectively), 10 µM kainate (green), and 10 µM kainate + 50 µM Cd (cyan) in an HEK cell transfected with GluK2(Q) L10C. Holding potential is −80 mV. **(B and C)** Plots of current variance versus mean current evoked by 10 µM kainate, 50 or 500 µM Cd alone, or 10 µM kainate plus 50 µM Cd in HEK cells expressing homomeric GluK2(Q) L10C (B) or GluK2(R) A8C (C). Note the variance data in A and B are from the same cell and plotted on the same variance scale, in A as a function of time and in B as a function of the mean current values for each time segment. Smooth curves in B are the best fits of the parabolic equation $\sigma^2 = i * I − (I^2/N)$, where σ^2 is variance, I is the mean macroscopic current, i is the unitary current (~0.1 pA), N is the number of channels (~12,000), and maximum $P_o = I_{max}/(i * N)$ (~0.5). Smooth curves in C are best straight line fits with slope = i (12 fA for kainate and 4 fA for 50 and 500 µM Cd).

For the A8C substitution, variance versus mean plots were essentially linear, suggesting a relatively low P_o (Lingle, 2006). In contrast to L10C, the slopes of GluK2 A8C variance versus mean plots were steeper for responses evoked by kainate than by 50 or 500 µM Cd, indicating a higher unitary conductance for channel activation by kainate (Fig. 7 and Table 3). Assuming that kainate and Cd act on the same number of channels, the higher maximal macroscopic current evoked by Cd reflects an ~20- to 30-fold higher open probability as compared with kainate: $(P_{o(Cd)}/P_{o(K)}) = (I_{Cd} * i_K)/(I_K * i_{Cd})$. In contrast, the unitary conductance for Cd alone was only 30–40% as large as for kainate (Table 3).

Specificity for Cys substitution and occlusion by MTS reagents
Cd and other metal ions can bind directly to Cys side chains (Holm et al., 1996; Rulíšek and Vondrášek, 1998) suggesting that Cys residues substituted at A8 or L10 may contribute to a novel Cd binding site. However, as mentioned above, residue changes at positions 8 and 10 (Fig. 5), as well as at a number of other M3 locations, can alter receptor properties even without exposure to metal ions (Kohda et al., 2000; Taverna et al., 2000; Klein and

Howe, 2004; Chang and Kuo, 2008), raising the possibility that conformational changes induced by substitutions in the bundle crossing might alter the effect of Cd binding elsewhere on the channel or expose novel cryptic Cd interaction sites that are not accessible in WT receptors. To determine whether activation by Cd required A8 replacement with Cys, we tested receptors in which A8 was substituted with other residues including Ser, Thr, Phe, and Tyr. As shown in Fig. 8, large inward currents evoked by exposure to 50 µM Cd alone (Fig. 8 A) or together with 10 µM kainate (Fig. 8 B) were only observed for receptors with A8C substitution. In addition, at higher doses (500 µM and 5 mM), Cd alone reduced the holding current and inhibited evoked current when coapplied with kainate to cells expressing the A8S, T, Y, or F substitution mutants (Fig. S2).

As a further test of the idea that Cd directly interacts with the Cys side chain substituted for A8 or L10, we compared the action of Cd before and after exposure to 100 µM MTSEA, a sulf-hydryl-reactive compound that modifies free cysteine residues to produce a positively charged side chain approximately the size of lysine (Fountain and North, 2006; Akabas, 2015). For both the A8C and L10C substitutions, treatment with MTSEA significantly reduced the amplitude of Cd-evoked current (Fig. 8, C–E). In the case of GluK2(Q) A8C, there was little effect on current evoked by kainate alone or on the holding current (Fig. 8 D), whereas for the L10C substitution, both the holding current and the current evoked by kainate were increased following exposure to MTSEA (Fig. 8, C and E). Thus, Cys modification by MTSEA reduces susceptibility to Cd activation of receptors with A8C or L10C substitutions.

Cd activation of heteromeric receptors
Homomeric mutant receptors with one M3 helix substitution per subunit would have a total of four novel introduced cysteines. To test whether Cys substitutions on all four subunits is required, we first evaluated the effects of Cd on heteromeric receptors produced in HEK cells cotransfected with mutant GluK2(Q) and WT GluK5 or GluK1(R). As shown in Fig. 9, cells cotransfected with either GluK1(R) or GluK5 together with GluK2(Q) A8C or GluK2(Q) L10C displayed currents that were activated by exposure to Cd alone as well as enhancement of KA-evoked current by Cd coapplication. Previous work suggests that formation of heteromeric receptors is strongly favored upon coexpression of GluK2 with GluK1 or GluK5 (Cui and Mayer, 1999; Wilding et al., 2005; Reiner et al., 2012); however, the possibility that sensitivity to Cd in these cells resulted from a minor population of homomeric GluK2(Q) A8C or L10C is difficult to rule out. Agonist- and Cd-evoked I-V relations displayed inward rectification for cells cotransfected with mutant GluK2(Q) and WT GluK5 (data not shown), which encodes a Gln at the Q/R site and does not undergo editing (Traynelis et al., 2010). In contrast, the I-V relations lacked inward rectification for cotransfections that included the GluK1(R) subunit (Fig. 9 B), supporting the heteromeric inclusion of edited GluK1(R) within Cd-sensitive receptors (Fig. 9, A and C). To provide additional evidence that activation by Cd does not require A8C or L10C substitution on all four subunits within the tetramer, we analyzed substitution mutants of chimeric subunits that only form functional receptors as coexpressed heteromers (Wilding et al., 2014).

Table 3. **Unitary parameters estimated from fluctuation analysis**

	Kainate	Cd	Cd	Kainate + Cd
	10 µM	50 µM	500 µM	10 + 50 µM
GluK2(Q) L10C				
Unitary current (fA)	92 ± 8	83 ± 13	76 ± 11	79 ± 9
Unitary conductance (pS)	1.15 ± 0.10	1.04 ± 0.16	0.94 ± 0.14	0.99 ± 0.11
g Cd/g K		0.93 ± 0.07	0.81 ± 0.05	0.85 ± 0.04
Maximal current (pA)	212 ± 38	75 ± 4	218 ± 18	412 ± 38
Open probability	0.21 ± 0.03	0.09 ± 0.02	0.30 ± 0.05	0.48 ± 0.03
P_o Cd/P_o K		0.4 ± 0.1	1.7 ± 0.5	3.9 ± 1.3
Number of cells	10	8	9	10
GluK2(R) A8C				
Unitary current (fA)	15.7 ± 3.0	4.4 ± 0.9	4.0 ± 0.7	
Unitary conductance (fS)	197 ± 37	55 ± 11	50 ± 9	
g Cd/g K		0.39 ± 0.07	0.32 ± 0.08	
Maximal current (pA)	473 ± 158	1,350 ± 300	860 ± 130	
P_o Cd/P_o K		27 ± 13	20 ± 6	
Number of cells	16	16	9	

Cys substitutions to chimeric subunits

Because NMDA receptors are obligate heteromers (Traynelis et al., 2010), chimeric subunits in which the GluK2(Q) TMD and CTD are linked with the ATD and LBD of GluN1 or GluN2B do not generate functional channels when expressed alone in HEK cells but only when coexpressed (Wilding et al., 2014). As shown in Fig. 10, 50 µM Cd alone activated chimeric receptors with A8C substitution to either the N2B/K2(Q) (Fig. 10 A) or N1/K2(Q) (Fig. 10 B) subunit or to both subunits (Fig. 10 C). In contrast, cells expressing chimeric receptors with WT M3 residues (Fig. 10 D) and cells transfected with WT GluN1 plus GluN2B (Fig. 10 E) often displayed small reductions in holding current when exposed to 50 µM Cd alone and partial block of agonist-evoked current, similar to the effects of Cd on WT GluK2 (Figs. 2 and 3). Fig. 10, F and G, summarize results for WT and A8C mutant chimeric subunits during exposure to Cd alone (Fig. 10 F) or Cd plus agonist (Fig. 10 G). When expressed as a fraction of the current evoked by agonist alone, responses to Cd alone or Cd plus agonist for chimeric receptors with A8C substitution to either the N1/K2(Q) or N2B/K2(Q) subunit were comparable to homomeric GluK2(Q) A8C and nearly as large as Cd responses observed for receptors with A8C substitution in both chimeric subunits (Fig. 10, F and G).

To test for possible differences in potency of Cd activation among chimeric receptors with either or both subunits bearing A8C substitutions, we evaluated the currents evoked by additional Cd concentrations. As shown in Figs. 10, A–C, and 11, A and B, exposure to Cd concentrations up to 50 µM yielded essentially monotonic current activation at the onset of Cd and monotonic decay on return to control solution. In contrast, currents elicited by higher Cd concentrations displayed a multiphasic time course characterized by an initial spike of inward current followed by

decay to a lower steady-state plateau and a prominent tail current on Cd wash out (Fig. 11 B), suggesting a composite response that includes a component of low-affinity block superimposed on current activation. For the summary plots in Fig. 11 D, the steady-state currents during Cd exposure are normalized to the maximal peak inward current recorded at the onset or offset of treatment with 5 mM Cd. Based on this analysis summarized in Table 1, Cd activation was more potent at receptors that included A8C substitutions in both chimeric subunits (EC_{50} = 5.6 ± 1.7 µM) than for receptors in which A8C was only present in the N2B/K2(Q) subunit (EC_{50} = 27 ± 9 µM) or the N1/K2(Q) subunit (EC_{50} = 47 ± 8 µM). In addition, block by higher Cd concentrations was substantially weaker for chimeric receptors that only included the A8C substitution to the N1/K2(Q) chimera (IC_{50} = 13 ± 10 mM; Fig. 11 A) but significantly more potent for chimeric receptors that included the N2B/K2(Q)A8C subunit, either alone (Fig. 11 B) or together with N1/K2(Q)A8C (IC_{50} = 1.1 ± 0.2 mM; Fig. 11 D). For comparison, we also evaluated the concentration dependence of Cd inhibition at WT N1 + N2B NMDA receptors as well as chimeric receptors with WT M3 residues. As shown in Fig. 12, inhibition observed during exposure to 10 µM NMDA and glycine was stronger for receptors lacking the A8C substitution, being half-maximal at 200 µM Cd for WT NMDA receptors and 400 µM for chimeric receptors.

As for homomeric GluK2 (Fig. 4 A, inset), we also used exponential fits to the monotonic rise and decay of current observed with exposure to 50 µM Cd to determine the onset and recovery time constants for current activation (Table 2). Kinetics of inhibition were estimated from the biphasic onset and recovery currents recorded upon exposure to high Cd concentrations, which were fit with the sum of two exponentials. Fig. 11 C shows an example for chimeric receptors that included N2B/K2(Q)A8C, expanded from the trace in Fig. 11 B, with the onset fit (red curve)
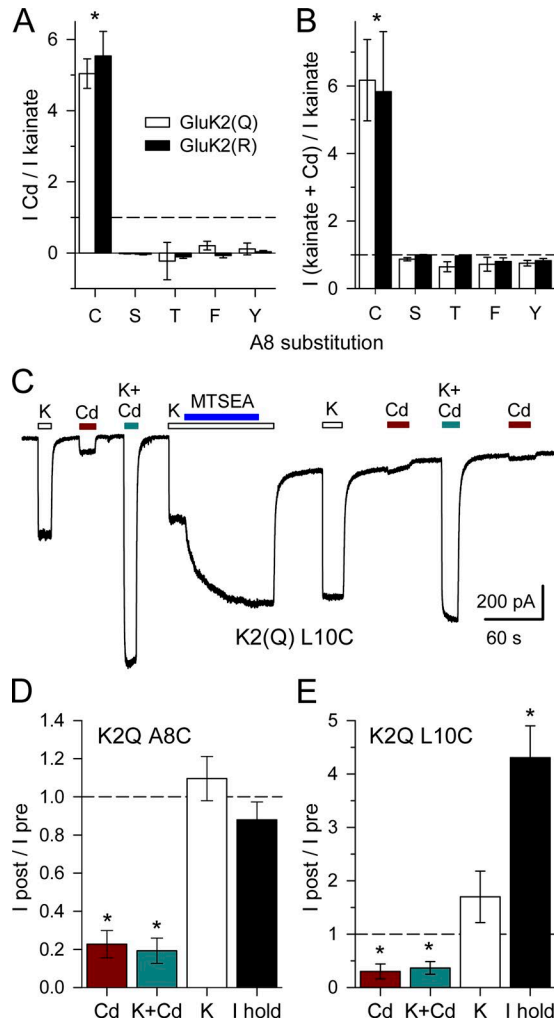
Figure 8. **Cd sensitivity requires Cys substitution. (A and B)** Summary plots of current (mean ± SEM) evoked by 50 µM Cd alone (A) or 10 µM kainate plus 50 µM Cd (B) as a fraction of current evoked by 10 µM kainate alone for A8 substitution with C, S, T, F, or Y. Asterisk denotes significant difference from S, T, F, or Y (ANOVA on ranks with post hoc Dunn's test, 5–114 [A] or 3–17 [B] cells per construct). **(C)** After brief exposure to 100 µM MTSEA (blue bar) together with 10 µM kainate (open bars), the holding current and current evoked by 10 µM kainate were increased, whereas current evoked by 50 µM Cd alone (red bars) or with 10 µM kainate (cyan bars) was reduced. **(D and E)** Summary plots of current (mean ± SEM) evoked by Cd alone or with kainate, by kainate alone, and the holding current after MTSEA as a fraction of current before MTSEA for GluK2(Q) A8C (D; six cells) or L10C (E; six cells). Asterisk denotes significant difference from I post = I pre (t statistic, P < 0.01).

Figure 9. **Cd activates heteromeric kainate receptors. (A)** Whole-cell currents evoked by 10 µM kainate (open bars) and 500 or 50 µM Cd alone (red bars) or together with 10 µM kainate (mauve and cyan bars, respectively) in a cell cotransfected with GluK2(Q) L10C and GluK1(R). **(B)** Lack of inward rectification in current–voltage relations from the same cell shown in A supports formation of heteromeric receptors. **(C)** Summary plots of current (mean ± SEM) evoked by 50 µM Cd alone (left; 10–114 cells per construct) or 50 µM Cd plus 10 µM kainate (right; 9–17 cells) as a fraction of kainate alone in cells transfected with GluK2(Q) alone or cotransfected with GluK2(Q) A8C or L10C together with either GluK1(R) or GluK5. Note the log scale. Asterisk denotes significant difference from homomeric GluK2(Q) A8C or L10C.

providing estimates for the time constant of current activation (τ_1) and block (τ_2) and the recovery fit (blue curve) yielding estimates for the time constant of unblock (τ_3) and deactivation (τ_4). We used the time constants determined for N1/K2 + N2B/K2 A8C (Table 2) to construct kinetic models (Fig. S3 and Table 3) that reproduce several features of Cd activation and block observed for the three chimeric subunit combinations analyzed in Fig. 11. The models assume that binding of either one or two Cd ions supports activation of receptors with A8C substitutions to both the N1/K2 and N2B/K2 subunits, whereas receptors with only one of the two chimeric subunits bearing an A8C mutation can only bind a single activating Cd. Inhibition is modeled by independent binding of up
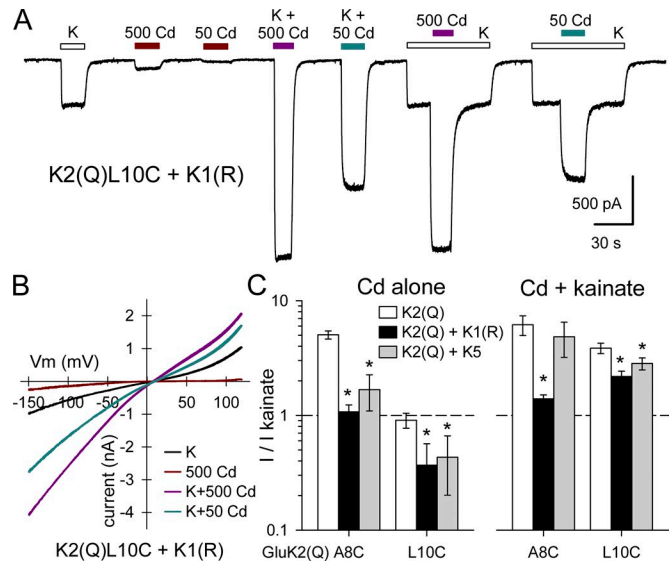
to four additional Cd ions to lower-affinity sites. The same set of rate constants for activation (k_{on} = 17,500 mol^{-1} s^{-1}, k_{off} = 0.39 s^{-1}), inhibition (k_{on} = 240 mol^{-1} s^{-1}, k_{off} = 2 s^{-1}), and channel opening (β = 50 s^{-1}, α = 200 s^{-1}) define the models for all three construct combinations: N1/K2 A8C + N2B/K2 (model 1 + 2), N1/K2 + N2B/K2 A8C (model 1 + 4), and N1/K2 A8C + N2B/K2 A8C (model 2 + 4).

As shown in Fig. 13, current activation by Cd alone and synergy between Cd and kainate was also observed for chimeric receptors with L10C substitutions to either the N1/K2(Q) or N2B/K2(Q) subunit or both. Comparing the results for receptors with A8C or L10C substitutions (Figs. 10 F and 13 B) confirmed a significantly larger effect by 50 µM Cd on receptors with Cys substitution to all four chimeric subunits in the tetramer (two-way ANOVA). For each of the construct combinations, however, post hoc pairwise comparison indicated no significant difference in 50 µM Cd effect between the A8C and the L10C substitution (Student–Newman–Keuls test). Collectively, the results in Figs. 10, 11, 12, and 13 confirm that substitution to all four subunits in the tetramer is not required for sensitivity to Cd at either the A8 or L10 positions. In addition, these experiments demonstrate similar activation by Cd for substitutions to either the N1/K2 or N2B/K2 chimeric subunits, suggesting nearly symmetrical interaction between subunits in either the A/C or B/D conformations, respectively (Wilding et al., 2014).

Mutation of potential coordination partners

The apparent potency of Cd activation of receptors with A8C substitutions in the 10–50 µM range (Fig. 10 D) is consistent with Cd
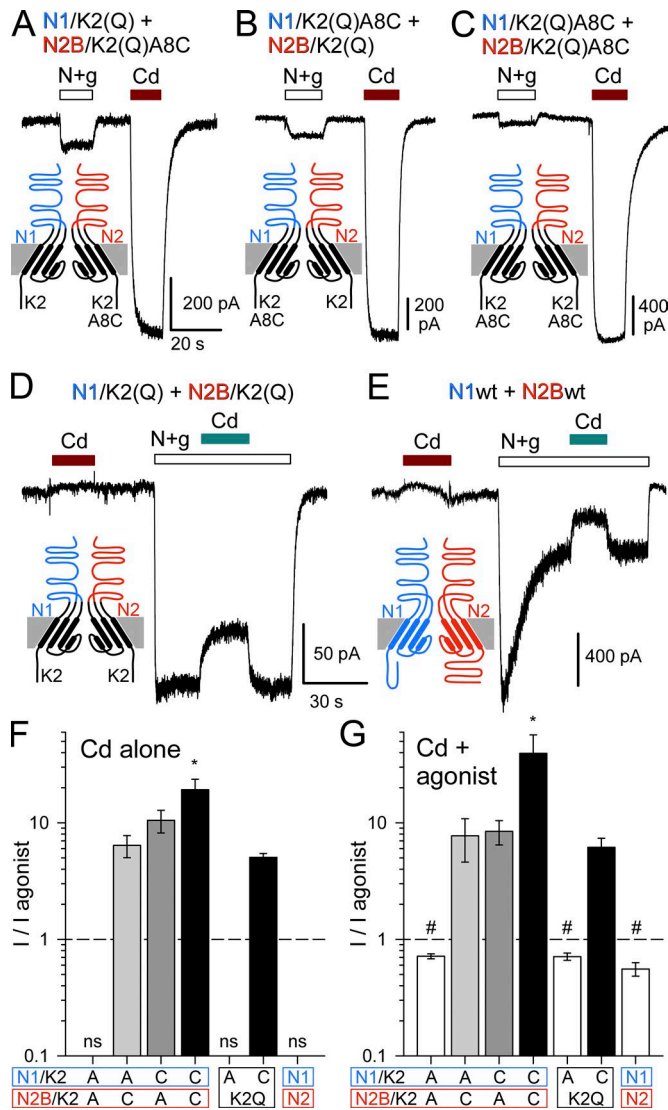
Figure 10. **Cadmium activation of chimeric receptors with A8C substitutions. (A–C)** Whole-cell currents evoked by 10 µM NMDA plus 10 µM glycine (open bars) or by 50 µM Cd alone (red bars) in HEK cells cotransfected with chimeric subunits bearing A8C substitutions on the N2B/K2(Q) subunit (A), on the N1/K2(Q) subunit (B), or on both chimeric subunits (C). **(D and E)** Chimeric receptors lacking cysteine substitution (D) and WT (N1 + N2B) NMDA receptors (E) were not activated by Cd alone, and coapplication of Cd (cyan bars) inhibited agonist-evoked current. **(F and G)** Summary plots of current evoked by Cd alone (F; 9–114 cells per construct) or together with agonists (G; 6–17 cells) as a fraction of the current evoked by agonists alone (mean ± SEM). The first four positions plot results for chimeric receptors. For comparison, GluK2(Q) WT and A8C results are replotted from Fig. 1 followed by WT GluN1 + GluN2B. Note the y-axis log scale. Asterisk denotes significantly greater effect of 50 µM Cd on receptors with A8C substitution to both chimeric subunits (one-way ANOVA with post hoc Student–Newman–Keuls test), # indicates significant inhibition of kainate-evoked current by Cd (t statistic), and ns indicates no significant increase in holding current by Cd alone (t statistic).

coordination by two or more side chains (Puljung and Zagotta, 2011; Zhou et al., 2015). The most likely coordination partners include His, Glu, Asp, or other Cys residues (Rulíšek and Vondrášek, 1998), although interactions involving other polar residues as well as backbone carbonyls are also possible. To test for potential coordination partners, we have begun making substitutions to
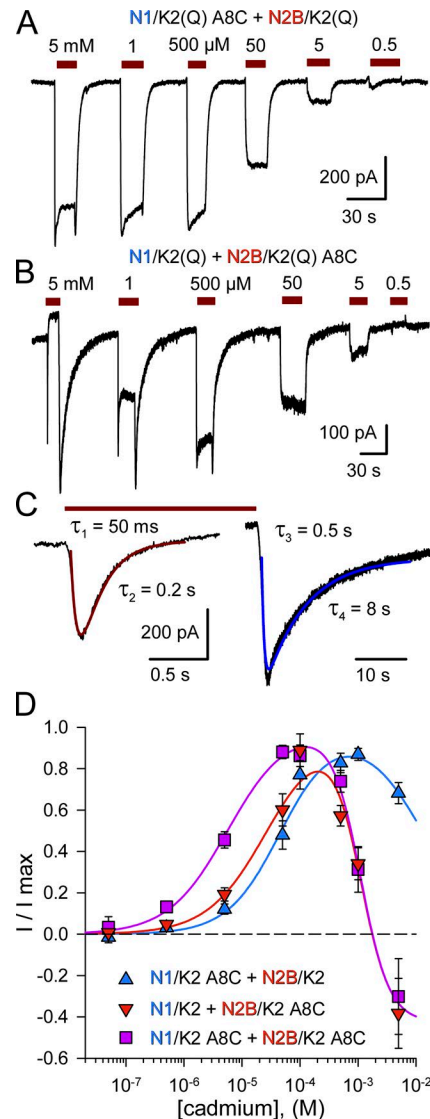

Figure 11. **Concentration dependence of chimeric A8C mutant receptor activation. (A and B)** Whole-cell currents evoked by Cd (5 and 1 mM and 500, 50, 5, and 0.5 µM) in cells transfected with N1/K2 A8C + N2B/K2 (A) or N1/K2 + N2B/K2 A8C (B). Chimeric receptors were both activated and blocked by the highest Cd doses tested, with stronger block observed for channels that included the N2B/K2 A8C subunit (B). **(C)** Currents from the onset and termination of 5 mM Cd exposure in B shown on an expanded time scale and fit with the sum of two exponentials (superimposed smooth curves). Exposure onset (red curve) includes time constants for activation ($\tau_1 = 50$ ms) and onset of block ($\tau_2 = 0.2$ s). On return to control solution (blue curve), receptors unblock ($\tau_3 = 0.5$ s) and deactivate ($\tau_4 = 8$ s). **(D)** Plot of steady-state current (mean ± SEM) during exposure to Cd as a fraction of the maximal Cd-evoked response, usually the peak tail current at termination of exposure to 5 mM Cd. Smooth curves are the best fit of (Materials and methods) $I/I_{max} = m + ((1/(1 + (EC_{50}/[Cd])^n) - m)/(1 + ([Cd]/IC_{50})^b))$. For N1/K2A8C + N2B/K2 (blue triangles; 14 cells) the $EC_{50} = 47 \pm 8$ µM, $n = 1.0 \pm 0.2$, $IC_{50} = 13 \pm 10$ mM, $b = 0.9 \pm 0.4$, and the minimum parameter (m) was set to zero. Curves for N1/K2 + N2B/K2A8C (red inverted triangles; 14 cells) and N1/K2A8C + N2B/K2A8C (violet squares; 21 cells) show simultaneous fits constrained to have the same $IC_{50} = 1.1 \pm 0.2$ mM, $b = 1.8 \pm 0.4$, $n = 0.9 \pm 0.1$, and $m = -0.43 \pm 0.12$ with different EC_{50} values 27 ± 9 µM and 5.6 ± 1.7 µM, respectively. Individual fits requiring three additional free parameters were not significantly better (F test).

likely candidate residues that are located near the A8 position in GluK2 homology models (Lopez et al., 2013) and cryo-EM structures
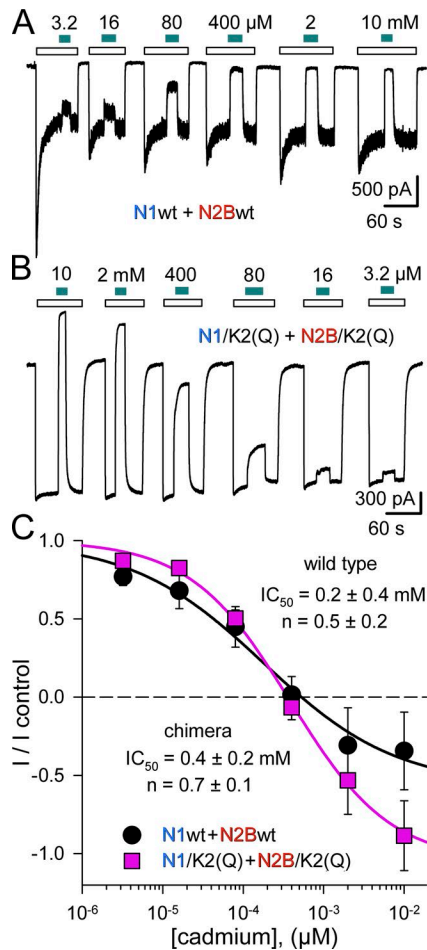
Figure 12. **Cd inhibits chimeric and WT NMDA receptors. (A and B)** Whole-cell currents evoked by 10 µM NMDA and 10 µM glycine (open bars) in HEK cells transfected with GluN1wt and GluN2Bwt cDNA (A) or with N1/K2(Q) and N2B/K2(Q) cDNA (B). Cd was coapplied at 3.2, 16, 80, or 400 µM or at 2 or 10 mM as indicated by the solid bars. **(C)** Current (mean ± SEM) recorded during Cd coapplication as a fraction of control current immediately before Cd exposure (six WT and eight chimera cells). Smooth curves are the best fit of $I/I_{control} = m + (1 - m)/(1 + ([Cd]/IC_{50})^n)$.

(Meyerson et al., 2016). There are no His residues near the GluK2 bundle crossing; therefore, our initial experiments focused on three negatively charged Glu residues in the S2–TMD linkers within 15 Å of the A8C side chain, as well as two Cys residues slightly farther away in the M1 helix. The plots in Fig. 14 show that activation by Cd persisted in receptors where these residues have been replaced individually or in combinations. Collectively, these results demonstrate that coordination of Cd between A8C and any of these side chains is not required for activation. Instead, coordination may involve neutral polar side chains, backbone carbonyl groups, or negatively charged residues more distant than 15 Å in currently available structures. Alternatively, Cd might coordinate between the substituted A8C side chains, although this would position Cd along the pore axis, which might be expected to impede ion flux (Discussion). Additional experiments will be needed to determine which of these various alternatives underlies coordination responsible for activation of A8C mutants by Cd.
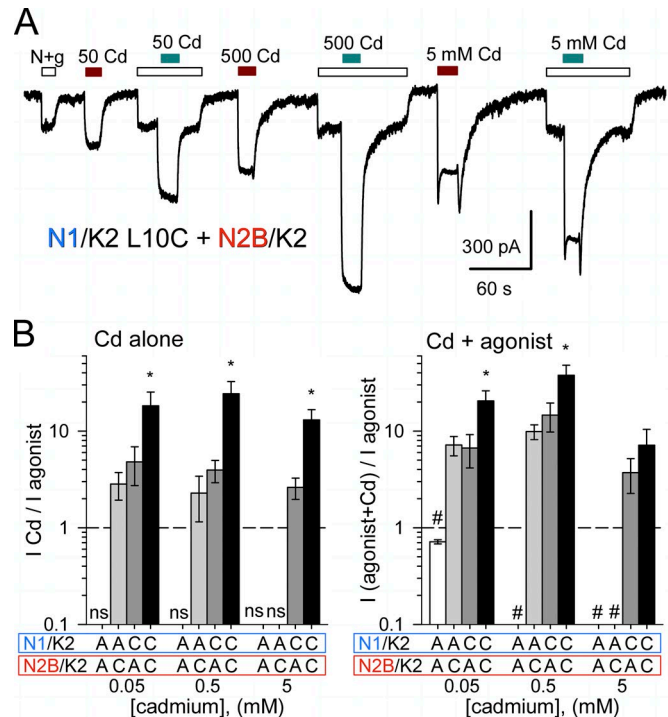

Figure 13. **Cd activation of chimeric receptors with L10C substitutions. (A)** Whole-cell currents activated by 10 µM NMDA plus 10 µM glycine (open bars) or 50 µM, 500 µM, or 5 mM Cd alone (red bars) or together with agonist (cyan bars). **(B)** Current (mean ± SEM) evoked by Cd alone (left; 5–15 cells per construct) or agonist plus Cd (right; 5–14 cells) as a fraction of current evoked by 10 µM NMDA plus 10 µM glycine. Note the y-axis log scale. Asterisk denotes significantly greater effect for receptors with L10C substitution to both chimeric subunits at each Cd dose (one-way ANOVA with post hoc Student–Newman–Keuls test), # indicates significant inhibition of kainate-evoked current by Cd (t statistic), and ns indicates no significant increase in holding current by Cd alone (t statistic).

Discussion

Recent work on iGluR gating has focused on the LBD–TMD linkers and the extracellular ends of the M1, M3, and M4 helices as loci for disease-causing mutations (Guzmán et al., 2017; Fry et al., 2018) and as targets for iGluR subtype-selective allosteric modulators (Yelshanskaya et al., 2016; Wang et al., 2017; Perszyk et al., 2018). The recognized importance of this region for control of channel gating has fueled recent mutagenesis work analyzing the structural requirements for mechanical coupling between the LBD and TMD (Alsaloum et al., 2016; Yelshanskaya et al., 2017; Ladislav et al., 2018). In the present study, we have identified two positions near the extracellular end of the M3 helix where cysteine substitution renders GluK2 kainate receptors susceptible to direct activation by exposure to Cd. One site is homologous to the location of the A8T point mutation in the iGluR delta subunit of Lurcher mice (Zuo et al., 1997; Kohda et al., 2000). The other site is a leucine located two residues farther along the M3 helix (L10), a rotation of 200° around the helical axis (Fig. 15 A). Our experiments demonstrate that strong activation by Cd is specific to Cys substitution and that exposure to Cys-reacting MTS reagents can occlude the effects of Cd. These results provide evidence that the introduced Cys residues directly interact with Cd but do not resolve whether coordination by additional side chains is required
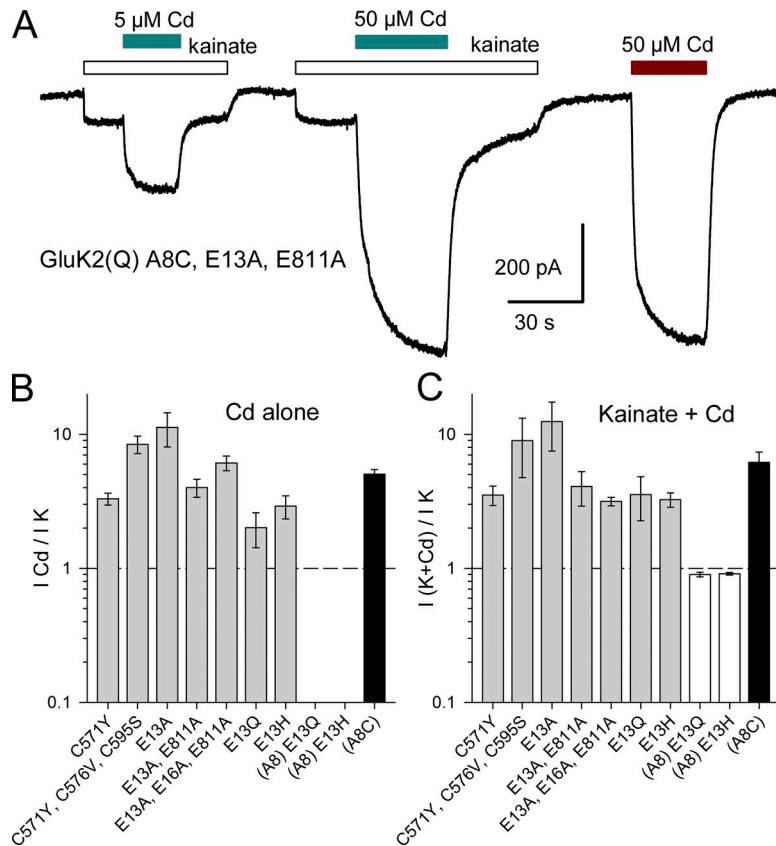
Figure 14. **Potential coordination partners not required for Cd activation. (A)** Whole-cell current 10 µM kainate (open bars), 50 µM Cd alone (red bar), and 5 or 50 µM Cd together with kainate (cyan bars) in an HEK cell transfected with triple mutant GluK2(Q) A8C, E13A (in the M3–S2 linker), and E811A (in the S2–M4 linker). **(B and C)** Summary plots of current (mean ± SEM) evoked by Cd alone (B; 4–114 cells per construct) or Cd plus kainate (C; 4–17 cells) as a fraction of the current evoked by kainate alone (note the y-axis log scale).

for channel activation. The difference in potency for Cd activation of channels with A8C or L10C substitutions suggests that distinct mechanisms may be involved. The EC_{50} values in the range of 5–10 µM that we observed for receptors with A8C substitutions on all four subunits are consistent with a Cd binding site involving at least two coordinating residues (Puljung and Zagotta, 2011), whereas the weaker potency for activation of homomeric GluK2(Q) L10C ($EC_{50} \sim 2$ mM) suggests that tight coordination by multiple residues is not required for Cd activation of channels bearing this mutation. For the L10C substitution, channel modification by MTSEA occluded activation by Cd but also produced changes that were similar to the effects observed during Cd exposure, including a substantial increase in the holding current as well as in kainate-evoked current. This result suggests that addition of positive charge at this location, which could serve to destabilize hydrophobic bundle crossing occlusion, has a similar effect on channel properties whether it results from the Cys side chain binding Cd or undergoing covalent modification by MTSEA. In contrast, for the A8C substitution, MTSEA occluded the action of Cd without significant change in holding current or activation by kainate, suggesting that addition of positive charge alone is not sufficient at this location and coordination by multiple residues may be necessary.

Previous work (Rulíšek and Vondrášek, 1998) indicates a bond length of ~2.6 Å between Cd ions and the terminal sulfur of Cys side chains, suggesting that other coordination partners would need to be relatively close to the A8C or L10C positions, at least in the Cd-bound activated state. Analysis of metal ion binding sites across a wide array of proteins (Holm et al., 1996; Rulíšek

and Vondrášek, 1998) suggests that the most likely coordination partners include histidine (Holmgren et al., 1998) or other free cysteine residues (Liu et al., 1997; Sobolevsky et al., 2002), as well as negatively charged glutamate or aspartate (Veran et al., 2012; Zhou et al., 2015), and with lower-frequency polar serine, threonine, or tyrosine residues or backbone carbonyls (Holm et al., 1996; Rulíšek and Vondrášek, 1998). As an initial screen for potential coordination partners, we generated substitutions that replaced Cys residues in the M1 helix or negatively charged Glu side chains in the M3–S2 and S2–M4 linkers within 15 Å of A8C; however, these changes failed to eliminate Cd activation of GluK2(Q) A8C, suggesting that these residues are not essential for direct coordination of Cd. Conformational changes associated with channel opening by Cd might bring other possible coordination partners within closer proximity of the A8C or L10C substitutions, but further experiments will be needed to determine whether any other residues more distant from the A8C or L10C are required.

Our results with heteromeric kainate receptors and receptors formed by coexpression of chimeric subunits demonstrate that activation by Cd does not require Cys substitution to all four subunits in the tetramer, although for the A8C substitution, Cd potency was shown to be lower for receptors with fewer M3 A8C replacements. Cd activated chimeric receptors with A8C substitutions in both the N1/K2 and N2B/K2 subunits with an EC_{50} of ~6 µM, which was similar to the EC_{50} of 10 µM observed for homomeric GluK2 A8C. In contrast, Cd was ~5- to 10-fold less potent for activation of chimeric receptors in which the A8C substitution was only present on the N2B/K2 ($EC_{50} = 27$ µM) or
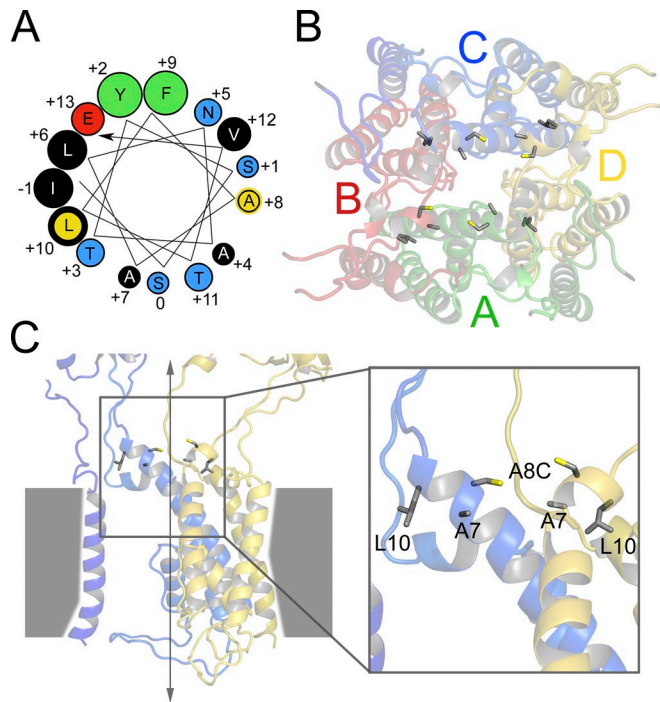
Figure 15. **The M3 helix positions that support activation by Cd. (A)** The M3 helical wheel from isoleucine (−1) to glutamate (+13). Circle diameters proportional to side chain volume. Colors denote side chain properties: negative charge (red), polar (blue), aromatic (green), hydrophobic (black), and cysteine substitution at positions 8 and 10 (yellow). **(B)** Semitransparent view down the open state model TMD axis illustrating A7, A8C, and L10 side chains. **(C)** The TMD side view of two GluK2 A8C open state homology model subunits in the C (blue) and D (yellow) conformations rotated 90° from B. The A7, A8C, and L10 side chains are shown as sticks. Vertical gray arrow denotes the central axis with the backbone cartoon semitransparent. A higher-resolution view of the boxed region is shown on the right.

the N1/K2 (EC$_{50}$ = 47 µM) subunit. Given that WT receptors show no activation for up to 5 mM Cd, we estimate a coupling energy (ΔΔG) of at least 3 kT (~1.9 kcal/mol) for A8C substitution of the two chimeric subunits.

Our numerical simulations suggest that relatively simple kinetic models are at least qualitatively consistent with activation and inhibition of chimeric receptors by Cd. The models include channel activation by binding one or two Cd ions depending on whether the A8C substitution was present on one or both of the GluN/GluK2 chimeric subunits, whereas inhibition results from two or four additional lower-affinity Cd binding steps. In the present case, state transitions in all of the models were defined by the same set of four rate constants, which corresponds to an assumption that all interactions are symmetrical and independent. Further simulations may provide a better quantitative fit to experimental recordings by modifying individual rate constants to incorporate positive or negative cooperativity between the various binding steps or to reflect possible asymmetry between A8C substitution to the N1/K2 or N2B/K2 chimeric subunits.

From previous work on block of GluA1 A7C AMPA receptors it has been suggested that metal ions can coordinate between introduced M3 Cys residues on adjacent subunits (Sobolevsky et al., 2004). Although this might explain Cd interaction with receptors that have Cys substitution in all four subunits of the tetramer,

it seems less likely to hold for heteromeric combinations with Cys substitution on only two of the four subunits. In particular, the N1–N2–N1–N2 alternating arrangement of native NMDA receptors (Salussolia et al., 2011; Riou et al., 2012; Karakas and Furukawa, 2014; Lee et al., 2014) predicts that our heteromeric chimeric receptors with A8C or L10C substitution in only the N1/K2 or only the N2B/K2 subunit would not present Cys residues on adjacent subunits but instead introduce Cys side chains displayed diagonally across the central axis with a separation distance of 12–14 Å in currently available closed and open state structures (Sobolevsky et al., 2009; Meyerson et al., 2016; Chen et al., 2017; Twomey et al., 2017). Although we cannot rule out coordination across the diagonal between Cys substitution to subunits in the A and C conformation (N1/K2 chimera) or the B and D conformation (N2B/K2 chimera), such a mechanism would appear to require substantial M3 reorientation and would locate the coordinated Cd ion directly along the central axis.

Recent work on the presumed open conformation of homomeric GluA2 AMPA receptors (Chen et al., 2017; Twomey et al., 2017) has described substantial deformations in the M3 helix of subunits in the B and D conformation with more limited changes to the A and C subunits. In particular, the M3 helix remains straight in the open state A and C conformations, whereas the B and D subunits exhibit a notable kink at the A4 position (Chen et al., 2017; Twomey et al., 2017), which precedes the A8C and L10C substitutions studied here. Fig. 15, B and C, depict axial and side views of a GluK2 A8C homology model based on the AMPA receptor open state structure. The A8C side chains reside closer to the pore axis than L10, which may contribute to the lower conductance ratios (g Cd/g K) observed for Cd bound to A8C compared with L10C. Although it remains to be determined whether M3 helix structural deformations occur in the open states of homomeric GluK2 or the GluN/GluK2 chimeric subunits, the modest functional asymmetry we observe for Cd activation and inhibition of A8C and L10C substitutions to N1/K2 or N2B/K2, together with the lower estimated unitary conductance for channels activated by Cd, suggest that the open states induced by Cd binding may be distinct from the native open conformation.

In contrast to cells transfected with WT GluK2, some of the cells expressing WT N1 + N2B or chimeric subunits with WT M3 residues displayed a reduction in holding current or inhibition beyond the initial holding level during exposure to millimolar Cd. For receptors bearing mutations that destabilize the bundle crossing, this effect at high Cd concentrations probably reflects inhibition of constitutive current mediated by the transfected receptors in the nominal absence of agonist. Our previous work (Wilding et al., 2014) showed that activation of receptors formed by chimeric subunits lacks the tight requirement for occupation of both NMDA and glycine sites observed with full-length WT subunits (Traynelis et al., 2010), suggesting that stray levels of glycine may be sufficient for chronic partial activation of chimeric receptors (Wilding et al., 2014). For cells transfected with WT NMDA receptor subunits, it remains to be determined whether all of the current blocked by millimolar Cd is mediated directly by NMDA receptors or whether expression of these receptors may enhance other Cd-sensitive currents, possibly by persistent elevation of cytoplasmic calcium levels.

Conclusions

Increasing evidence implicates a role for kainate receptors in nociception (Bhangoo and Swanson, 2013) and neural development (Guzmán et al., 2017) as well as neuropathologies including epilepsy (Crépel and Mulle, 2015) and psychiatric disorders (Lerma and Marques, 2013). Better understanding of how these receptors operate should aid in the design of therapeutic agents. Our experiments demonstrate that Cd binding can directly open channels with Cys substitutions at two positions near the inner helix bundle crossing, circumventing the requirement for agonist site occupation. At one of the sites (L10C), Cd binding acts synergistically with agonist, and tight coordination of Cd is not required. In contrast, we saw no evidence for synergy with agonist for channel activation by Cd coordination at the A8C substitution two residues preceding L10. The A8 position is homologous to the delta subunit residue where gain of function mutations produce cerebellar ataxia both in humans (Coutelier et al., 2015) and in the Lurcher mutant mouse strain (Zuo et al., 1997). More recently, de novo A8T mutation in human *GRIK2*, which encodes the GluK2 subunit, was shown to underlie a set of human neurodevelopmental deficits including ataxia and intellectual disability (Guzmán et al., 2017). Additional work on M3 helix substitutions should help further elucidate the conformational changes that mediate iGluR gating in health and disease.

Acknowledgments

References

Akabas, M.H. 2015. Cysteine modification: Probing channel structure, function and conformational change. *Adv. Exp. Med. Biol.* 869:25–54. https://doi.org/10.1007/978-1-4939-2845-3_3

Alsaloum, M., R. Kazi, Q. Gan, J. Amin, and L.P. Wollmuth. 2016. A molecular determinant of subtype-specific desensitization in ionotropic glutamate receptors. *J. Neurosci.* 36:2617–2622. https://doi.org/10.1523/JNEUROSCI.2667-15.2016

Bean, B.P., C.A. Williams, and P.W. Ceelen. 1990. ATP-activated channels in rat and bullfrog sensory neurons: Current-voltage relation and single-channel behavior. *J. Neurosci.* 10:11–19. https://doi.org/10.1523/JNEUROSCI.10-01-00011.1990

Beck, C., L.P. Wollmuth, P.H. Seeburg, B. Sakmann, and T. Kuner. 1999. NMDAR channel segments forming the extracellular vestibule inferred from the accessibility of substituted cysteines. *Neuron.* 22:559–570. https://doi.org/10.1016/S0896-6273(00)80710-2

Bhangoo, S.K., and G.T. Swanson. 2013. Kainate receptor signaling in pain pathways. *Mol. Pharmacol.* 83:307–315. https://doi.org/10.1124/mol.112.081398

Chang, H.R., and C.C. Kuo. 2008. The activation gate and gating mechanism of the NMDA receptor. *J. Neurosci.* 28:1546–1556. https://doi.org/10.1523/JNEUROSCI.3485-07.2008

Chen, S., Y. Zhao, Y. Wang, M. Shekhar, E. Tajkhorshid, and E. Gouaux. 2017. Activation and desensitization mechanism of AMPA receptor-TARP complex by Cryo-EM. *Cell.* 170:1234–1246.e14. https://doi.org/10.1016/j.cell.2017.07.045

Coutelier, M., L. Burglen, E. Mundwiller, M. Abada-Bendib, D. Rodriguez, S. Chantot-Bastaraud, C. Rougeot, M.A. Cournelle, M. Milh, A. Toutain, et al. 2015. GRID2 mutations span from congenital to mild adult-onset cerebellar ataxia. *Neurology.* 84:1751–1759. https://doi.org/10.1212/WNL.0000000000001524

Crépel, V., and C. Mulle. 2015. Physiopathology of kainate receptors in epilepsy. *Curr. Opin. Pharmacol.* 20:83–88. https://doi.org/10.1016/j.coph.2014.11.012

Cui, C., and M.L. Mayer. 1999. Heteromeric kainate receptors formed by the coassembly of GluR5, GluR6, and GluR7. *J. Neurosci.* 19:8281–8291. https://doi.org/10.1523/JNEUROSCI.19-19-08281.1999

Doyle, D.A., J. Morais Cabral, R.A. Pfuetzner, A. Kuo, J.M. Gulbis, S.L. Cohen, B.T. Chait, and R. MacKinnon. 1998. The structure of the potassium channel: Molecular basis of K+ conduction and selectivity. *Science.* 280:69–77. https://doi.org/10.1126/science.280.5360.69

Eswar, N., D. Eramian, B. Webb, M.Y. Shen, and A. Sali. 2008. Protein structure modeling with MODELLER. *Methods Mol. Biol.* 426:145–159. https://doi.org/10.1007/978-1-60327-058-8_8

Fernández-Marmiesse, A., H. Kusumoto, S. Rekarte, I. Roca, J. Zhang, S.J. Myers, S.F. Traynelis, M.L. Couce, L. Gutierrez-Solana, and H. Yuan. 2018. A novel missense mutation in GRIN2A causes a nonepileptic neurodevelopmental disorder. *Mov. Disord.* 33:992–999. https://doi.org/10.1002/mds.27315

Fountain, S.J., and R.A. North. 2006. A C-terminal lysine that controls human P2X4 receptor desensitization. *J. Biol. Chem.* 281:15044–15049. https://doi.org/10.1074/jbc.M600442200

Fry, A.E., K.A. Fawcett, N. Zelnik, H. Yuan, B.A.N. Thompson, L. Shemer-Meiri, T.D. Cushion, H. Mugalaasi, D. Sims, N. Stoodley, et al. 2018. De novo mutations in GRIN1 cause extensive bilateral polymicrogyria. *Brain.* 141:698–712. https://doi.org/10.1093/brain/awx358

Gleitsman, K.R., S.M. Kedrowski, H.A. Lester, and D.A. Dougherty. 2008. An intersubunit hydrogen bond in the nicotinic acetylcholine receptor that contributes to channel gating. *J. Biol. Chem.* 283:35638–35643. https://doi.org/10.1074/jbc.M807226200

Guzmán, Y.F., K. Ramsey, J.R. Stolz, D.W. Craig, M.J. Huentelman, V. Narayanan, and G.T. Swanson. 2017. A gain-of-function mutation in the *GRIK2* gene causes neurodevelopmental deficits. *Neurol. Genet.* 3:e129. https://doi.org/10.1212/NXG.0000000000000129

Hille, B. 2001. Ion Channels of Excitable Membranes. Third edition. Sinauer Associates, Sunderland, MA.

Holm, R.H., P. Kennepohl, and E.I. Solomon. 1996. Structural and functional aspects of metal sites in biology. *Chem. Rev.* 96:2239–2314. https://doi.org/10.1021/cr9500390

Holmgren, M., K.S. Shin, and G. Yellen. 1998. The activation gate of a voltage-gated K+ channel can be trapped in the open state by an intersubunit metal bridge. *Neuron.* 21:617–621. https://doi.org/10.1016/S0896-6273(00)80571-1

Howe, J.R. 1996. Homomeric and heteromeric ion channels formed from the kainate-type subunits GluR6 and KA2 have very small, but different, unitary conductances. *J. Neurophysiol.* 76:510–519. https://doi.org/10.1152/jn.1996.76.1.510

Huettner, J.E. 2015. Glutamate receptor pores. *J. Physiol.* 593:49–59. https://doi.org/10.1113/jphysiol.2014.272724

Huettner, J.E., E. Stack, and T.J. Wilding. 1998. Antagonism of neuronal kainate receptors by lanthanum and gadolinium. *Neuropharmacology.* 37:1239–1247. https://doi.org/10.1016/S0028-3908(98)00082-3

Jones, K.A., T.J. Wilding, J.E. Huettner, and A.M. Costa. 1997. Desensitization of kainate receptors by kainate, glutamate and diastereomers of 4-methylglutamate. *Neuropharmacology.* 36:853–863. https://doi.org/10.1016/S0028-3908(97)00066-X

Jones, K.S., H.M. VanDongen, and A.M. VanDongen. 2002. The NMDA receptor M3 segment is a conserved transduction element coupling ligand binding to channel opening. *J. Neurosci.* 22:2044–2053. https://doi.org/10.1523/JNEUROSCI.22-06-02044.2002

Karakas, E., and H. Furukawa. 2014. Crystal structure of a heterotetrameric NMDA receptor ion channel. *Science.* 344:992–997. https://doi.org/10.1126/science.1251915

Kash, T.L., A. Jenkins, J.C. Kelley, J.R. Trudell, and N.L. Harrison. 2003. Coupling of agonist binding to channel gating in the GABA(A) receptor. *Nature.* 421:272–275. https://doi.org/10.1038/nature01280

Klein, R.M., and J.R. Howe. 2004. Effects of the lurcher mutation on GluR1 desensitization and activation kinetics. *J. Neurosci.* 24:4941–4951. https://doi.org/10.1523/JNEUROSCI.0660-04.2004

Kohda, K., Y. Wang, and M. Yuzaki. 2000. Mutation of a glutamate receptor motif reveals its role in gating and delta2 receptor channel properties. *Nat. Neurosci.* 3:315–322. https://doi.org/10.1038/73877

Ladislav, M., J. Cerny, J. Krusek, M. Horak, A. Balik, and L. Vyklicky. 2018. The LILI motif of M3-S2 linkers is a component of the NMDA receptor channel gate. *Front. Mol. Neurosci.* 11:113. https://doi.org/10.3389/fnmol.2018.00113

Lee, C.H., W. Lü, J.C. Michel, A. Goehring, J. Du, X. Song, and E. Gouaux. 2014. NMDA receptor structures reveal subunit arrangement and pore architecture. *Nature.* 511:191–197. https://doi.org/10.1038/nature13548

Lerma, J., and J.M. Marques. 2013. Kainate receptors in health and disease. *Neuron.* 80:292–311. https://doi.org/10.1016/j.neuron.2013.09.045

Li, D., H. Yuan, X.R. Ortiz-Gonzalez, E.D. Marsh, L. Tian, E.M. McCormick, G.J. Kosobucki, W. Chen, A.J. Schulien, R. Chiavacci, et al. 2016. GRIN2D recurrent de novo dominant mutation causes a severe epileptic encephalopathy treatable with NMDA receptor channel blockers. *Am. J. Hum. Genet.* 99:802–816. https://doi.org/10.1016/j.ajhg.2016.07.013

Lingle, C.J. 2006. Empirical considerations regarding the use of ensemble-variance analysis of macroscopic currents. *J. Neurosci. Methods.* 158:121–132. https://doi.org/10.1016/j.jneumeth.2006.05.027

Liu, Y., M. Holmgren, M.E. Jurman, and G. Yellen. 1997. Gated access to the pore of a voltage-dependent K+ channel. *Neuron.* 19:175–184. https://doi.org/10.1016/S0896-6273(00)80357-8

Lopez, M.N., T.J. Wilding, and J.E. Huettner. 2013. Q/R site interactions with the M3 helix in GluK2 kainate receptor channels revealed by thermodynamic mutant cycles. *J. Gen. Physiol.* 142:225–239. https://doi.org/10.1085/jgp.201311000

Mah, S.J., E. Cornell, N.A. Mitchell, and M.W. Fleck. 2005. Glutamate receptor trafficking: Endoplasmic reticulum quality control involves ligand binding and receptor function. *J. Neurosci.* 25:2215–2225. https://doi.org/10.1523/JNEUROSCI.4573-04.2005

Mayer, M.L. 2017. The Challenge of Interpreting Glutamate-Receptor Ion-Channel Structures. *Biophys. J.* 113:2143–2151. https://doi.org/10.1016/j.bpj.2017.07.028

Meyerson, J.R., S. Chittori, A. Merk, P. Rao, T.H. Han, M. Serpe, M.L. Mayer, and S. Subramaniam. 2016. Structural basis of kainate subtype glutamate receptor desensitization. *Nature.* 537:567–571. https://doi.org/10.1038/nature19352

Mott, D.D., M. Benveniste, and R.J. Dingledine. 2008. pH-dependent inhibition of kainate receptors by zinc. *J. Neurosci.* 28:1659–1671. https://doi.org/10.1523/JNEUROSCI.3567-07.2008

Murthy, S.E., T. Shogan, J.C. Page, E.M. Kasperek, and G.K. Popescu. 2012. Probing the activation sequence of NMDA receptors with lurcher mutations. *J. Gen. Physiol.* 140:267–277. https://doi.org/10.1085/jgp.201210786

Perszyk, R., B.M. Katzman, H. Kusumoto, S.A. Kell, M.P. Epplin, Y.A. Tahirovic, R.L. Moore, D. Menaldino, P. Burger, D.C. Liotta, and S.F. Traynelis. 2018. An NMDAR positive and negative allosteric modulator series share a binding site and are interconverted by methyl groups. *eLife.* 7:e34711. https://doi.org/10.7554/eLife.34711

Puljung, M.C., and W.N. Zagotta. 2011. Labeling of specific cysteines in proteins using reversible metal protection. *Biophys. J.* 100:2513–2521. https://doi.org/10.1016/j.bpj.2011.03.063

Reiner, A., R.J. Arant, and E.Y. Isacoff. 2012. Assembly stoichiometry of the GluK2/GluK5 kainate receptor complex. *Cell Reports.* 1:234–240. https://doi.org/10.1016/j.celrep.2012.01.003

Riou, M., D. Stroebel, J.M. Edwardson, and P. Paoletti. 2012. An alternating GluN1-2-1-2 subunit arrangement in mature NMDA receptors. *PLoS One.* 7:e35134. https://doi.org/10.1371/journal.pone.0035134

Rulíšek, L., and J. Vondrášek. 1998. Coordination geometries of selected transition metal ions (Co2+, Ni2+, Cu2+, Zn2+, Cd2+, and Hg2+) in metalloproteins. *J. Inorg. Biochem.* 71:115–127. https://doi.org/10.1016/S0162-0134(98)10042-9

Salussolia, C.L., M.L. Prodromou, P. Borker, and L.P. Wollmuth. 2011. Arrangement of subunits in functional NMDA receptors. *J. Neurosci.* 31:11295–11304. https://doi.org/10.1523/JNEUROSCI.5612-10.2011

Schmid, S.M., C. Körber, S. Herrmann, M. Werner, and M. Hollmann. 2007. A domain linking the AMPA receptor agonist binding site to the ion pore controls gating and causes lurcher properties when mutated. *J. Neurosci.* 27:12230–12241. https://doi.org/10.1523/JNEUROSCI.3175-07.2007

Schwarz, M.K., V. Pawlak, P. Osten, V. Mack, P.H. Seeburg, and G. Köhr. 2001. Dominance of the lurcher mutation in heteromeric kainate and AMPA receptor channels. *Eur. J. Neurosci.* 14:861–868. https://doi.org/10.1046/j.0953-816x.2001.01705.x

Sigworth, F.J. 1980. The variance of sodium current fluctuations at the node of Ranvier. *J. Physiol.* 307:97–129. https://doi.org/10.1113/jphysiol.1980.sp013426

Sobolevsky, A.I., L. Rooney, and L.P. Wollmuth. 2002. Staggering of subunits in NMDAR channels. *Biophys. J.* 83:3304–3314. https://doi.org/10.1016/S0006-3495(02)75331-9

Sobolevsky, A.I., M.V. Yelshansky, and L.P. Wollmuth. 2004. The outer pore of the glutamate receptor channel has 2-fold rotational symmetry. *Neuron.* 41:367–378. https://doi.org/10.1016/S0896-6273(04)00008-X

Sobolevsky, A.I., M.L. Prodromou, M.V. Yelshansky, and L.P. Wollmuth. 2007. Subunit-specific contribution of pore-forming domains to NMDA receptor channel structure and gating. *J. Gen. Physiol.* 129:509–525. https://doi.org/10.1085/jgp.200609718

Sobolevsky, A.I., M.P. Rosconi, and E. Gouaux. 2009. X-ray structure, symmetry and mechanism of an AMPA-subtype glutamate receptor. *Nature.* 462:745–756. https://doi.org/10.1038/nature08624

Swartz, K.J., W.J. Koroshetz, A.H. Rees, and J.E. Huettner. 1992. Competitive antagonism of glutamate receptor channels by substituted benzazepines in cultured cortical neurons. *Mol. Pharmacol.* 41:1130–1141.

Taverna, F., Z.G. Xiong, L. Brandes, J.C. Roder, M.W. Salter, and J.F. MacDonald. 2000. The Lurcher mutation of an alpha-amino-3-hydroxy-5-methyl-4-isoxazolepropionic acid receptor subunit enhances potency of glutamate and converts an antagonist to an agonist. *J. Biol. Chem.* 275:8475–8479. https://doi.org/10.1074/jbc.275.12.8475

Traynelis, S.F., L.P. Wollmuth, C.J. McBain, F.S. Menniti, K.M. Vance, K.K. Ogden, K.B. Hansen, H. Yuan, S.J. Myers, and R. Dingledine. 2010. Glutamate receptor ion channels: Structure, regulation, and function. *Pharmacol. Rev.* 62:405–496. https://doi.org/10.1124/pr.109.002451

Twomey, E.C., and A.I. Sobolevsky. 2018. Structural mechanisms of gating in ionotropic glutamate receptors. *Biochemistry.* 57:267–276. https://doi.org/10.1021/acs.biochem.7b00891

Twomey, E.C., M.V. Yelshanskaya, R.A. Grassucci, J. Frank, and A.I. Sobolevsky. 2017. Channel opening and gating mechanism in AMPA-subtype glutamate receptors. *Nature.* 549:60–65. https://doi.org/10.1038/nature23479

Venkatachalan, S.P., and C. Czajkowski. 2008. A conserved salt bridge critical for GABA(A) receptor function and loop C dynamics. *Proc. Natl. Acad. Sci. USA.* 105:13604–13609. https://doi.org/10.1073/pnas.0801854105

Veran, J., J. Kumar, P.S. Pinheiro, A. Athané, M.L. Mayer, D. Perrais, and C. Mulle. 2012. Zinc potentiates GluK3 glutamate receptor function by stabilizing the ligand binding domain dimer interface. *Neuron.* 76:565–578. https://doi.org/10.1016/j.neuron.2012.08.027

Wang, T.M., B.M. Brown, L. Deng, B.D. Sellers, P.J. Lupardus, H.J.A. Wallweber, A. Gustafson, E. Wong, M. Volgraf, J.B. Schwarz, et al. 2017. A novel NMDA receptor positive allosteric modulator that acts via the transmembrane domain. *Neuropharmacology.* 121:204–218. https://doi.org/10.1016/j.neuropharm.2017.04.041

Wilding, T.J., Y. Zhou, and J.E. Huettner. 2005. Q/R site editing controls kainate receptor inhibition by membrane fatty acids. *J. Neurosci.* 25:9470–9478. https://doi.org/10.1523/JNEUROSCI.2826-05.2005

Wilding, T.J., E. Fulling, Y. Zhou, and J.E. Huettner. 2008. Amino acid substitutions in the pore helix of GluR6 control inhibition by membrane fatty acids. *J. Gen. Physiol.* 132:85–99. https://doi.org/10.1085/jgp.200810009

Wilding, T.J., K. Chen, and J.E. Huettner. 2010. Fatty acid modulation and polyamine block of GluK2 kainate receptors analyzed by scanning mutagenesis. *J. Gen. Physiol.* 136:339–352. https://doi.org/10.1085/jgp.201010442

Wilding, T.J., M.N. Lopez, and J.E. Huettner. 2014. Radial symmetry in a chimeric glutamate receptor pore. *Nat. Commun.* 5:3349:1–10. https://doi.org/10.1038/ncomms4349

Wollmuth, L.P., T. Kuner, C. Jatzke, P.H. Seeburg, N. Heintz, and J. Zuo. 2000. The Lurcher mutation identifies δ 2 as an AMPA/kainate receptor-like channel that is potentiated by Ca(2+). *J. Neurosci.* 20:5973–5980. https://doi.org/10.1523/JNEUROSCI.20-16-05973.2000

Yelshanskaya, M.V., A.K. Singh, J.M. Sampson, C. Narangoda, M. Kurnikova, and A.I. Sobolevsky. 2016. Structural bases of noncompetitive inhibition of AMPA-subtype ionotropic glutamate receptors by antiepileptic drugs. *Neuron.* 91:1305–1315. https://doi.org/10.1016/j.neuron.2016.08.012

Yelshanskaya, M.V., S. Mesbahi-Vasey, M.G. Kurnikova, and A.I. Sobolevsky. 2017. Role of the ion channel extracellular collar in AMPA receptor gating. *Sci. Rep.* 7:1050:1–12. https://doi.org/10.1038/s41598-017-01146-z

Yuan, H., K. Erreger, S.M. Dravid, and S.F. Traynelis. 2005. Conserved structural and functional control of N-methyl-D-aspartate receptor gating by transmembrane domain M3. *J. Biol. Chem.* 280:29708–29716. https://doi.org/10.1074/jbc.M414215200

Zhou, Y., X.M. Xia, and C.J. Lingle. 2015. Cadmium-cysteine coordination in the BK inner pore region and its structural and functional implications. *Proc. Natl. Acad. Sci. USA.* 112:5237–5242. https://doi.org/10.1073/pnas.1500953112

Zuo, J., P.L. De Jager, K.A. Takahashi, W. Jiang, D.J. Linden, and N. Heintz. 1997. Neurodegeneration in Lurcher mice caused by mutation in delta2 glutamate receptor gene. *Nature.* 388:769–773. https://doi.org/10.1038/42009